The Plant Cell, Vol. 24: 3921–3948, October 2012, www.plantcell.org

LARGE-SCALE BIOLOGY ARTICLE

Systems and *Trans*-System Level Analysis Identifies Conserved Iron Deficiency Responses in the Plant Lineage[W][OA]

Eugen I. Urzica,[a] David Casero,[b,c] Hiroaki Yamasaki,[a,c] Scott I. Hsieh,[a] Lital N. Adler,[a] Steven J. Karpowicz,[a,1] Crysten E. Blaby-Haas,[a] Steven G. Clarke,[a] Joseph A. Loo,[a,c,d] Matteo Pellegrini,[b,c] and Sabeeha S. Merchant[a,c,2]

[a] Department of Chemistry and Biochemistry, University of California, Los Angeles, California 90095
[b] Department of Molecular, Cell, and Developmental Biology, University of California, Los Angeles, California 90095
[c] Institute of Genomics and Proteomics, David Geffen School of Medicine at the University of California, Los Angeles, California 90095
[d] Department of Biological Chemistry, David Geffen School of Medicine at the University of California, Los Angeles, California 90095

We surveyed the iron nutrition-responsive transcriptome of *Chlamydomonas reinhardtii* using RNA-Seq methodology. Presumed primary targets were identified in comparisons between visually asymptomatic iron-deficient versus iron-replete cells. This includes the known components of high-affinity iron uptake as well as candidates for distributive iron transport in *C. reinhardtii*. Comparison of growth-inhibited iron-limited versus iron-replete cells revealed changes in the expression of genes in chloroplastic oxidative stress response pathways, among hundreds of other genes. The output from the transcriptome was validated at multiple levels: by quantitative RT-PCR for assessing the data analysis pipeline, by quantitative proteomics for assessing the impact of changes in RNA abundance on the proteome, and by cross-species comparison for identifying conserved or universal response pathways. In addition, we assessed the functional importance of three target genes, *VITAMIN C 2* (*VTC2*), *MONODEHYDROASCORBATE REDUCTASE 1* (*MDAR1*), and *CONSERVED IN THE GREEN LINEAGE AND DIATOMS 27* (*CGLD27*), by biochemistry or reverse genetics. VTC2 and MDAR1, which are key enzymes in de novo ascorbate synthesis and ascorbate recycling, respectively, are likely responsible for the 10-fold increase in ascorbate content of iron-limited cells. CGLD27/At5g67370 is a highly conserved, presumed chloroplast-localized pioneer protein and is important for growth of *Arabidopsis thaliana* in low iron.

INTRODUCTION

Iron is an essential nutrient for virtually all life forms because of its broad function as a catalyst, particularly of redox reactions and reactions involving O_2 chemistry. Iron is found in two stable oxidation states, Fe(II) or Fe(III), associated directly with ligands from amino acid side chains in proteins as in mononuclear iron in iron superoxide dismutase or di-iron enzymes like acyl-acyl carrier protein desaturases and methane mono-oxygenases or assembled into organic and inorganic cofactors like hemes or iron-sulfur centers. The redox potentials and reactivities of iron proteins are determined by the number and type of coordinating ligands.

Despite its abundance on earth, iron has limited bioavailability because of its relative insolubility in the Fe(III) oxidation state, which is the prevalent form in most aerobic environments (Guerinot and Yi, 1994; Staiger, 2002). Accordingly, iron metabolism uses transport systems involving chelation and redox chemistry (often multiple sequential steps) followed by biosynthesis of heme, inorganic Fe/S, or other clusters (Theil, 2004; Lill and Mühlenhoff, 2008; Philpott and Protchenko, 2008; Kosman, 2010). In eukaryotic cells, there is the additional complication of subcellular compartmentation and delivery of iron or assembled cofactors across membranes, and this is exacerbated in plants where the plastid is yet another compartment (Jeong and Guerinot, 2009). In multicellular organisms, transport from sites of assimilation (roots or gastrointestinal tract) to sites of utilization (leaves, muscle, or reticulocytes) involves redox chemistry and chelation as well (Hellman and Gitlin, 2002; De Domenico et al., 2008; Morrissey and Guerinot, 2009; Schultz et al., 2010).

Nevertheless, despite the occurrence of sophisticated acquisition mechanisms, organisms can be chronically undernourished for iron, as evidenced by high prevalence of anemia worldwide and by iron limitation of primary productivity (Morel et al., 1991; Hell and Stephan, 2003; Benoist et al., 2008; Behrenfeld et al., 2009). We and others have used *Chlamydomonas reinhardtii* as a reference organism for understanding the impact of poor iron nutrition on bioenergetic pathways in plants and acclimation mechanisms (Merchant et al., 2006; Clemens et al., 2009).

C. reinhardtii, a chlorophyte alga, is usually grown in the laboratory photoautotrophically (in the presence of light and CO_2) in defined medium containing the required mineral nutrients or photoheterotrophically (in the presence of light and acetate) where the availability of a reduced carbon source precludes a requirement for photosynthesis (Harris, 2009). Interestingly,

[1] Current address: Department of Biology, University of Central Oklahoma, Edmond, OK 73034.
[2] Address correspondence to sabeeha@chem.ucla.edu.
The author responsible for distribution of materials integral to the findings presented in this article in accordance with the policy described in the Instructions for Authors (www.plantcell.org) is: Sabeeha S. Merchant (sabeeha@chem.ucla.edu).
[W] Online version contains Web-only data.
[OA] Open Access articles can be viewed online without a subscription.
www.plantcell.org/cgi/doi/10.1105/tpc.112.102491

some molecular responses to iron deficiency are connected to metabolic demand. Specifically, the iron-rich photosynthetic apparatus is dispensable in low iron, acetate-containing medium but is maintained in iron-poor, CO_2-grown cells (Naumann et al., 2007; Terauchi et al., 2010). The loss of photosynthetic complexes occurs by programmed degradation of the chlorophyll protein complexes, starting with disconnection of the photosystem I (PSI) antenna (light-harvesting complex I) and followed by the loss of PSI, the light-harvesting complex I antenna proteins, and photosystem II (La Fontaine et al., 2002; Moseley et al., 2002; Naumann et al., 2005). The abundances of the respiratory complexes are unchanged in acetate-grown cells. Other responses, such as upregulation of iron assimilation, are less dependent on the mode of growth, and we used the expression pattern of iron-uptake components as an indicator of iron nutritional status (La Fontaine et al., 2002).

Specifically, we defined three operational stages of iron nutrition: the iron-replete situation, corresponding to ~20 μM iron in standard *C. reinhardtii* medium; the iron-deficient situation, corresponding to 1 to 3 μM iron, where classical iron deficiency chlorosis is not evident, but the expression of *FOX1* (a sentinel gene for poor iron nutrition, encoding a multicopper oxidase involved in high-affinity transport) is dramatically upregulated; and the iron-limited situation, corresponding to ≤0.5 μM iron, where the growth of cells is inhibited because of insufficient nutritional supply of iron (Merchant et al., 2006). Reporter gene assays established that the change in expression of genes *FEA1*, *FOX1*, and *FTR1*, encoding various iron assimilation components, occurs at the level of transcription, indicating that comparative transcriptomics might reveal new components of the nutritional iron regulon (Allen et al., 2007a; Deng and Eriksson, 2007; Fei et al., 2009, 2010). To distinguish primary responses, we compared iron-sufficient to asymptomatic iron-deficient cells under photoautotrophic as well as photoheterotrophic conditions, and to distinguish the impact of poor iron nutrition on various stress response pathways, we included iron-limited cells. A parallel comparison of the proteome indicated excellent positive correlation between changes in RNA and protein abundance for a subset of differentially expressed genes, suggesting that these are mechanistically important for acclimation, and negative correlation for RNAs encoding iron binding proteins, suggesting that these changes represent a feedback response to the loss of function of the corresponding proteins.

To identify responses that might be specific for chloroplast biology, we surveyed previously published microarray data for iron deficiency responses in two other evolutionarily distant organisms in the plant lineage: *Arabidopsis thaliana* and rice (*Oryza sativa*). A comparison revealed a set of responses shared with *C. reinhardtii*, including a few plastid proteins. Functional tests of two genes, *MONODEHYDROASCORBATE REDUCTASE 1* (*MDAR1*) and *CONSERVED IN THE GREEN LINEAGE AND DIATOMS 27* (*CGLD27*), by biochemistry and reverse genetics indicated their relevance for growth in iron-poor conditions.

RESULTS

The Iron Assimilation Pathway Is a Sentinel of Cellular Iron Status

Cells of wild-type strain 2137 (CC-4532) were grown under illumination in batch culture in standard Tris-phosphate medium with or without acetate supplementation and with different amounts of iron supplementation (Figure 1). As noted previously, when acetate is available for photosynthesis-independent growth, the cells sacrifice the photosynthetic apparatus, evident by a nearly 75% decrease in chlorophyll content and reduced F_v/F_m (Moseley et al., 2002; Terauchi et al., 2010). In the absence of acetate, the loss of chlorophyll is less dramatic and photochemical activity is maintained. To distinguish pathways of acclimation of iron deficiency in the context of iron utilization for bioenergetic membranes in respiration versus photosynthesis, we sought

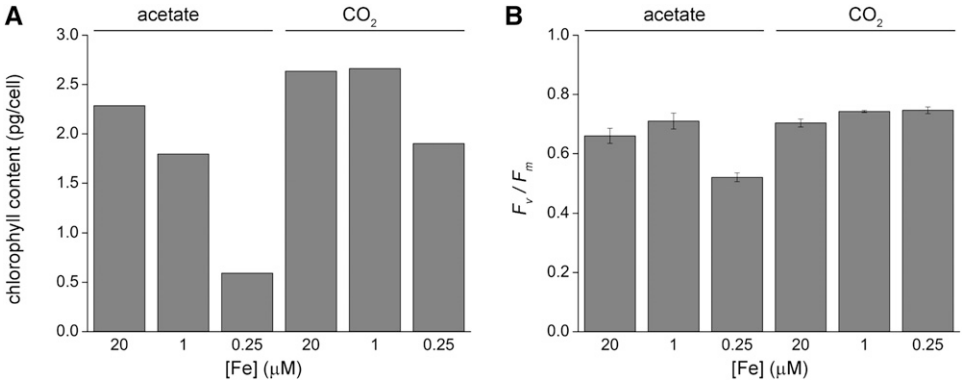

Figure 1. Iron Limitation Has a Major Effect on Photosynthesis in Photoheterotrophically Grown *C. reinhardtii* Cells.

(A) Total chlorophyll content of photoheterotrophic versus photoautotrophic cells. Cells were grown in the presence of acetate or CO_2 in various concentrations of iron (replete, deficient, and limited), and chlorophyll abundance was measured as described in Methods.

(B) Maximum quantum efficiency of photosystem II in photoheterotrophic versus photoautotrophic cells in response to iron nutrition. *C. reinhardtii* cells were grown in iron-replete, iron-limited, and iron-deficient media, and chlorophyll fluorescence was analyzed in liquid cultures as described in Methods. Error bars represent the SD from three biological replicates.

to describe the *C. reinhardtii* iron deficiency transcriptome in both the presence and absence of acetate in the growth medium.

In previous work, we found that cells in fully iron-replete medium consume 3 μM iron (out of 20 μM) by the time they reach stationary phase (>10^7 cells mL^{-1}), corresponding to luxury consumption (Page et al., 2012). Nevertheless, when they are iron-limited, they can manage with much less through the activation of iron-sparing responses, corresponding to economical consumption (Merchant and Helmann, 2012). Therefore, in medium containing low micromolar amounts of iron, the cells transition from luxury uptake and utilization to an iron economy mode. We used the expression of genes in the iron assimilation pathway (La Fontaine et al., 2002; Allen et al., 2007a) as sentinels or markers of iron status as cells inoculated into medium containing various amounts of iron (corresponding to limited, deficient, and replete) progressed through lag and log phase to stationary phase (Figure 2).

The *FOX1*, *FRE1*, *IRT1*, and *FEA1* genes are expressed at very low levels in replete medium (20 μM). In medium containing 1 μM iron, these genes are more highly expressed. For *FOX1*, *FRE1*, and *FEA1*, there is a marginal increase in RNA abundance as iron content is reduced below 1 μM, and this pattern is recapitulated in the protein profile for the ferroxidase (Figure 2B). As continued growth and division further depletes iron from the medium, expression increases further (cf. each set of points and see particularly the *IRT1* gene). At iron concentrations that limit growth (≤0.5 μM iron), the sentinel genes are highly expressed shortly after inoculation, even at low cell densities; the responses at 0.25 μM are stronger than at 0.5 μM. These results reinforce the importance of intracellular iron content and quota. Therefore, we chose 20, 1, and 0.25 μM iron to generate replete, deficient, and limited cells, respectively. Because of the effect of cell density on iron status and, hence, gene expression, we sampled each culture at the same cell density (of 3×10^6 cells mL^{-1}) so that externally supplied iron is a proxy for intracellular iron availability (Figure 3).

Total RNA was analyzed by sequencing cDNAs on the Illumina GAIIx platform. Between 0.7 and 1 Gb of 35-nucleotide sequences (and 2 to 3 Gb of 100-nucleotide sequences) were obtained from each sample and aligned to the *C. reinhardtii* draft genome (version 4, Augustus 10.2 annotation) (Stanke et al., 2008; http://www.phytozome.net/chlamy) as described previously (Urzica et al., 2012). Approximately 90% of all reads align to the genome, and from those, 70 to 75% aligned uniquely to the Augustus 10.2 gene models (see Supplemental Data Set 1 online, first sheet). Note that the Augustus 10.2 annotation was compiled with support from ~2 Gb of 454 reads derived from RNA isolated from various conditions, including iron deficiency (http://genomes.mcdb.ucla.edu/Cre454/). Therefore, this set of gene models is likely to include most of the genes in the iron regulon. Expression estimates for each gene model in each sample were calculated as described previously (Urzica et al., 2012) and are provided in units of reads per kilobase of exons in each model per million of aligned reads (RPKMs) (see Supplemental Data Set 1 online, second sheet) (Mortazavi et al., 2008).

Two Principal Components

We rationalized that a comparison of replete (20 μM) to asymptomatic (1 μM) iron-deficient cells would reveal direct responses to reduced iron availability, whereas comparisons of replete and deficient to iron-limited conditions (0.25 μM) would reveal second-stage or secondary mechanisms involved in coping with sustained or prolonged iron limitation (Figure 3A; see Supplemental Data Sets 2 and 3 online, three sheets each). Comparisons of differentially accumulating RNAs in photoautotrophic versus photoheterotrophic conditions should illuminate the impact of photosynthesis switching from an essential to a dispensable pathway (see Supplemental Figure 1 and Supplemental Data Set 4 online, 10 sheets).

Principal component analysis of the data from all experiments indicates that the first principal component groups the data by growth medium, revealing, not surprisingly, that carbon source is a much more important determinant of genome-wide pattern of expression relative to iron nutrition, which is the second component by which the data are grouped (Figure 3B). The analysis shows a much tighter distribution of the iron-limited data with the iron-deficient and iron-replete from photoautotrophically grown cells, consistent with less dramatic phenotypic differences (Figure 1), whereas the data from iron-limited photoheterotrophic cells are more distinct compared with the data from iron-deficient and iron-replete conditions, again consistent with the strong phenotypes (Figure 1; Terauchi et al., 2010).

For the functional classification of iron deficiency responses, we chose genes whose expression level is higher than the median level of expression (based on RPKMs) and that are at least twofold differentially expressed with a false discovery rate (FDR) <5%. In acetate-grown cells (photoheterotrophic), we found that 78 and 2050 genes were differentially expressed in iron-deficient and iron-limited cells, respectively (Figure 3C, comparing set A with B). Out of the 2050 genes regulated under iron limitation, 1286 showed greater mRNA abundance (referred to subsequently as induced, regardless of the underlying mechanism), whereas 764 genes had reduced transcript abundance (referred to subsequently as repressed). Under iron deficiency, from the total of 78 differentially expressed genes, most (74) were upregulated (Figure 3D). Most of the differentially expressed genes in the iron-limited photoheterotrophic cells (1976 out of 2050) were unique to the limitation condition, while only a handful of differentially regulated genes (four of 78) were unique to the deficiency situation (Figures 3C and 3D). The majority of the differentially regulated genes in iron deficiency then were differentially regulated under both conditions (1 and 0.25 μM iron), consistent with the premise in the experimental design, and suggesting that these 74 genes are primary targets of nutritional iron signaling in photoheterotrophic conditions (Figure 3C, intersection of comparison A-B; see Supplemental Data Set 2 online).

Many fewer genes were affected by iron nutrition under photoautotrophic conditions (0.04% CO_2): 35 and 422 genes differentially expressed (greater than or equal to twofold change, FDR < 5%) in iron-deficient and iron-limited conditions, respectively (Figure 3C, comparison C-D; see Supplemental Data Set 3 online). As for the photoheterotrophically grown cells, most of the changes that occurred in iron deficiency were observed also in the iron-limited data set (33 out of 35). For 45 genes, regulation was verified by real-time RT-PCR on an

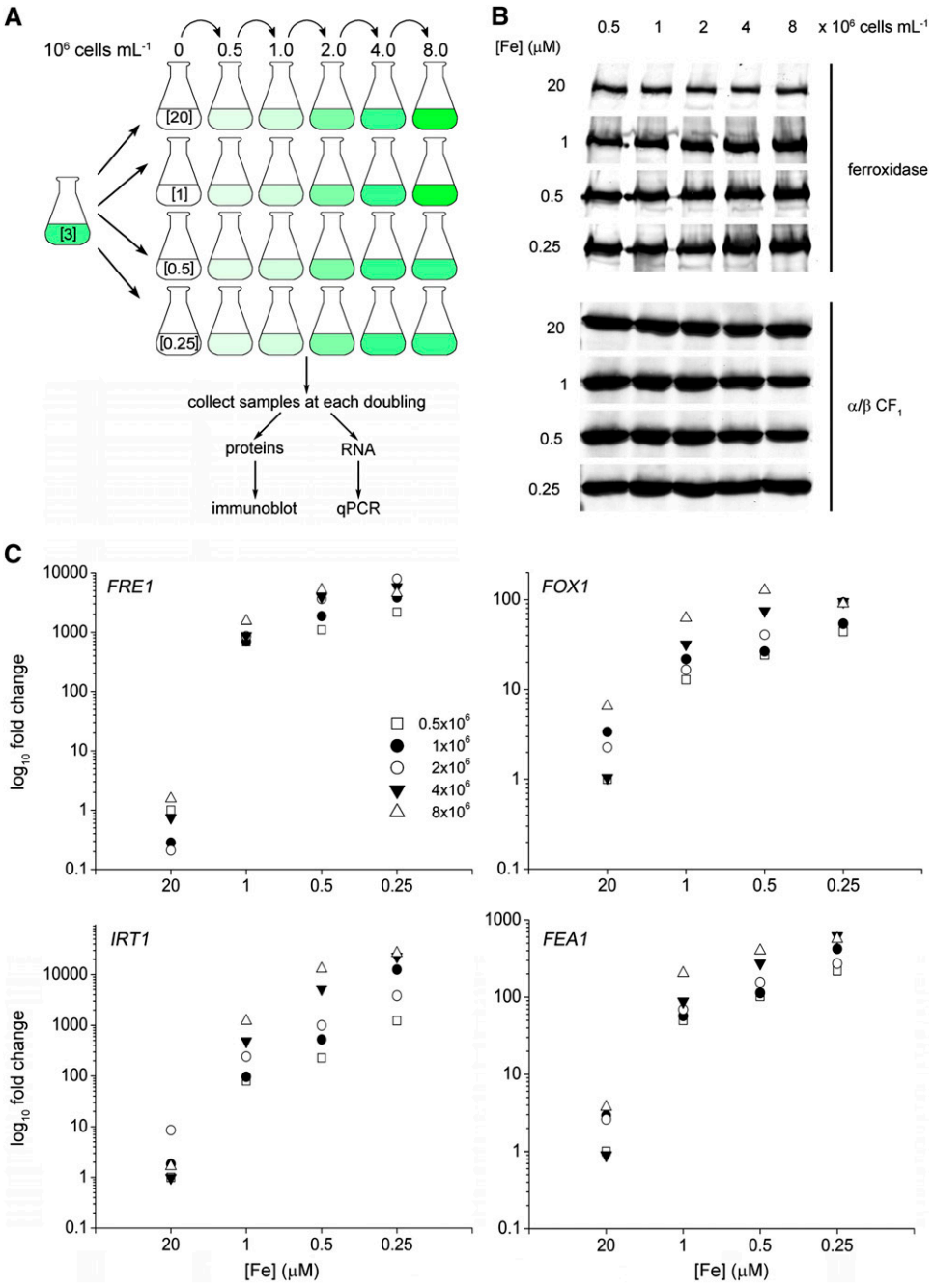

Figure 2. Iron Nutrition–Dependent Expression of Genes Encoding Components of Iron Assimilation Pathways.

(A) Schematic representation of the experiment. Briefly, *C. reinhardtii* cells grown photoheterotrophically in iron-replete conditions (3 μM iron) to a cell density of 2×10^6 cells mL^{-1} were used to inoculate cultures containing different iron concentrations (representing replete [20], deficient [1], and limited [0.25] and [0.5] with concentrations in μM) to a cell density of 10^4 cells mL^{-1}. Samples were collected for biochemical analyses at the indicated cell densities corresponding to early, mid, late logarithmic, and stationary phases. qPCR, quantitative PCR.

(B) Ferroxidase abundance in response to iron nutrition and cell density. Twenty micrograms of total membrane protein was separated by denaturing PAGE and transferred to a membrane, which was probed with antibodies against ferroxidase and CF_1.

(C) Expression of marker genes for iron nutritional status is increased at early stages of photoheterotrophic growth. Expression of sentinel genes was analyzed by quantitative real-time PCR. Fold change was calculated according to the $2^{-\Delta\Delta C_T}$ (cycle threshold) method (Livak and Schmittgen, 2001).

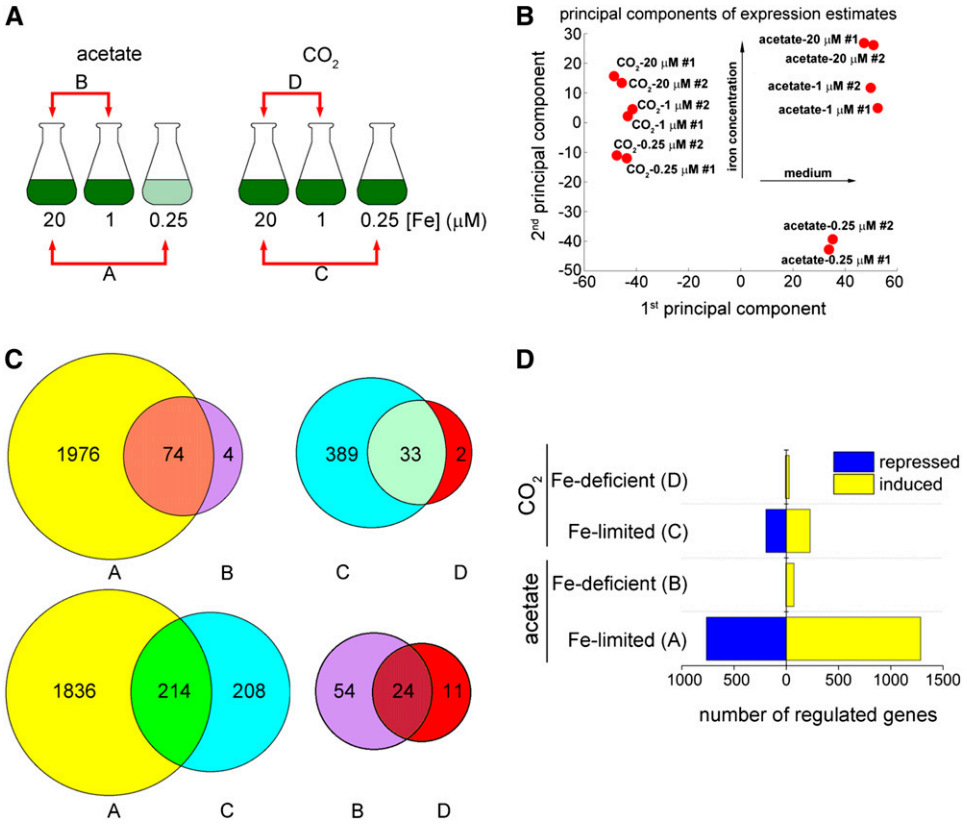

Figure 3. Identification of Iron Nutrition–Responsive Genes.

C. reinhardtii cells were grown photoheterotrophically (acetate) or photoautotrophically (CO_2) under iron-replete (20 μM iron), iron-deficient (1 μM iron), and iron-limited (0.25 μM iron) conditions. Cells were collected at a density of 3×10^6 cells mL^{-1}.

(A) Illustration of growth conditions and of comparisons A, B, C, and D. The pale-green color depicted for iron-limited conditions indicates that the cells are chlorotic.

(B) Principal component analysis of the transcriptome groups the experiments based first on carbon source (first principal component) and then on iron levels (second principal component).

(C) The Venn diagrams show the differentially expressed genes identified (fold change ≥ 2, FDR <5%). The numbers in the intersections represent the genes revealed in two comparisons.

(D) Induced (yellow) or repressed (blue) genes under photoheterotrophic (acetate) and photoautotrophic (CO_2) iron-deficient and iron-limited conditions. The correspondence between each set of bars and the relevant comparison in **(B)** are indicated in parentheses.

independent set of RNA samples (see Supplemental Figure 2 online).

Functional Classification Emphasizes Transporters and Stress Responses

The set of 78 genes in comparison B (Figure 3A) representing the primary iron deficiency response includes those encoding assimilatory iron transport components (FTR1, FEAs, IRTs, and ferroxidase) and candidates (NRAMP4, Cre02.g099500, which is an ortholog of yeast Ccc1p/*Arabidopsis* VIT1, and Cre16.g687000, a ferroportin-like molecule) for intracellular/distributive iron transport, together constituting 17% of the iron deficiency regulon (13 of 78 genes) (Figures 4A and 4B, left panel, Table 1). Another notable set (25%) is the category of redox and stress proteins, indicative of a marked effect of low iron nutrition on cellular redox chemistry. Several of the genes in this category encode iron binding proteins like ferredoxins 3/6 and chloroplast DnaJ-domain proteins CDJ3/5, whose RNAs are increased in iron-deficient cells (Terauchi et al., 2009; Dorn et al., 2010; Table 2). By contrast, mRNAs for ferredoxin 2 are reduced in abundance. Since ferredoxin 2 is required for nitrate assimilation, its decrease may be part of an iron-sparing response: the protein would be less necessary in ammonium-grown cells (Terauchi et al., 2009).

About 7% of differentially regulated genes under iron-deficient conditions encode proteins involved in signaling or involved in nucleic acid metabolism, whereas around 9% of differentially expressed genes encode proteins involved in other cellular processes (Figures 4A and 4B, left panel). Three genes (4%) encode proteins related to cell structure and function. A similar distribution of functional categories was observed when we analyzed the proteins differentially expressed under photoautotrophic iron deficiency (Figures 4A and 4B, right panels).

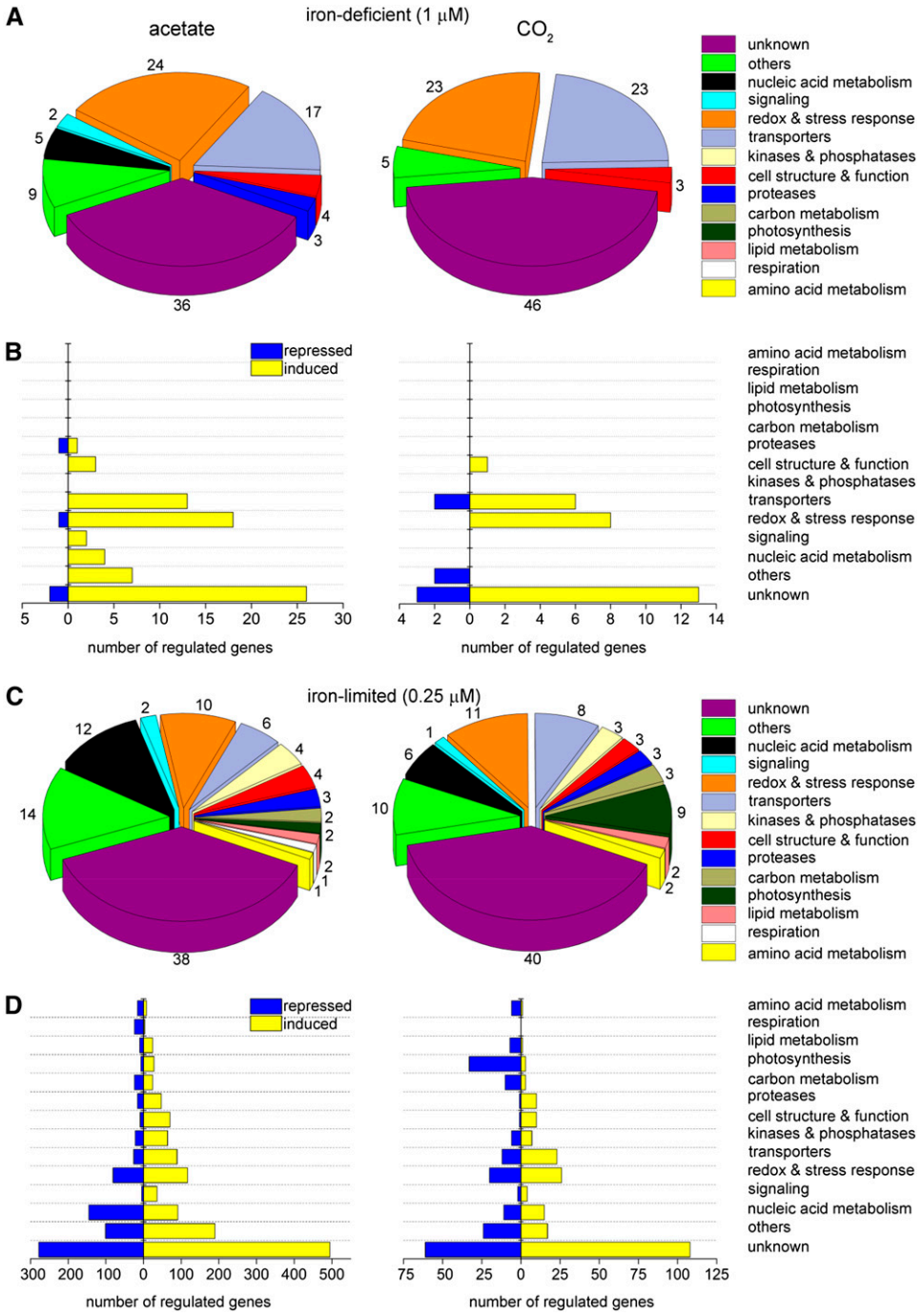

Figure 4. Similar Pathways Are Affected by Iron Nutrition in CO_2- versus Acetate-Grown Cells.

The deduced protein sequences from comparisons B (78 genes) (**[A]** and **[B]**, left panels), D (35 genes) (**[A]** and **[B]**, right panels), A (2050 genes) (**[C]** and **[D]**, left panels), and C (422 genes) (**[C]** and **[D]**, right panels) were analyzed at the Pfam site (E-value 10^{-4}) and/or by BLASTp analysis at NCBI or Phytozome. The protein domains were grouped according to their function in 14 categories: unknown, other, nucleic acid metabolism, signaling, redox and stress response, transporters, kinases and phosphatases, cell structure and function, proteases, carbon metabolism, photosynthesis, lipid metabolism, respiration, and amino acid metabolism. Unknowns refer to protein sequences for which a domain could not be identified or if the domain was identified as having an unknown function (DUF). Domains that could not be classified in any specific category were grouped into the "others" category. The numbers outside pie charts depict how much (in percentage) each functional category is represented in the total numbers of differentially expressed transcripts from each individual set of data.

Table 1. Effect of Low Iron Nutrition on Abundance of RNAs Encoding Components of Iron Assimilation and Metabolism and Antioxidant and Signaling Pathways in Photoheterotrophic Cells

			RPKM			Fold Change	
Process	Gene[a]	Defline	20[b]	1[b]	0.25[b]	1/20	0.25/20
Fe Homeostasis	*FRE1*	Ferric-chelate reductase/ oxidoreductase	0.18	895	3140	4972	17444
	IRT1	Iron nutrition–responsive ZIP family transporter	nd	1.2	204	14	2048
	FEA2	Iron-assimilating protein 2	6.9	378	2762	55	400
	NRAMP4	Natural resistance-associated macrophage domain protein	4.9	46	189	9.4	39
	FTR1	Iron permease	38	324	1264	8.5	33
	IRT2	Iron nutrition–responsive ZIP family transporter	3.5	30	60	8.6	17
	TEF22	DOMON domain; cytochrome b_{561}/ferric reductase domain	51	384	841	7.5	16
	FEA1	Iron-assimilating protein 1	248	2417	3629	9.7	15
	Cre05.g241400	Putative ferric reductase-like transmembrane component	13	76	175	5.8	13
	Cre02.g107550	Similar to yeast CCC1 and plant VIT1	11	25	95	2.3	8.6
	FOX1	Multicopper ferroxidase	178	795	1386	4.5	7.8
	Cre16.g687000	Similar to ferroportin	6.7	22	51	3.3	7.6
	Cre02.g099500	Similar to yeast CCC1 and plant VIT1	22	32	56	1.5	2.5
Antioxidants	*FER2*	Ferritin subunit	0.05	7.1	65	142	1300
	MSD3	Superoxide dismutase (Mn)	1.0	43	546	43	546
	PCS1	Phytochelatin synthase	3.8	26	125	6.8	33
	MDAR1	Monodehydroascorbate reductase	45	214	1255	4.8	28
	GRX6	Glutaredoxin, CGFS type	43	62	496	1.4	12
	VTC2	GDP-galactose:glucose-1-phosphate guanyltransferase	19	47	195	2.5	10
	FER1	Ferritin subunit	276	918	1694	3.3	6.1
	GPX3	Glutathione peroxidase	2.5	3.8	10	1.5	4.0
	TRX16	Putative thioredoxin	6.7	9.7	35	1.4	5.2
	GSH1	γ-Glutamylcysteine synthetase	39	72	212	1.8	5.4
	Cre01.g031500	Putative ascorbate oxidase	4.2	6.3	15	1.5	3.6
	PRX6	Thioredoxin dependent peroxidase	12	8.7	45	0.7	3.8
	Cre11.g471150	Peroxiredoxin; alkyl hydroperoxide reductase	6.4	8.7	21	1.4	3.3
	TRX15	Thioredoxin-like protein	20	18	66	0.9	3.3
	LIPA2	Lipoic acid synthetase	12	13	31	1.1	2.6
	GST10	Glutathione *S*-transferase	68	90	175	1.3	2.6
	TRX17	Thioredoxin-like protein	20	18	46	0.9	2.3
	CDSP32	Plastidic thioredoxin-like protein	88	88	43	1.0	0.5
	CAT1	Catalase/peroxidase	204	183	96	0.9	0.5
	TRX11	Putative plastidic thioredoxin-like protein	24	19	8.6	0.8	0.4
	GPX5	Glutathione peroxidase	177	139	59	0.8	0.3
	CITRX	Thioredoxin-related protein CITRX	128	127	39	1.0	0.3
	CAT2	Catalase/peroxidase	19	23	5.6	1.2	0.3
	LIPB	Lipoate protein ligase	4.0	1.2	1.0	0.3	0.3
	GST6	Predicted protein with glutathione *S*-transferase domain	26	25	3.2	1.0	0.1
Transcriptional Regulators	*MYB4*	Myb-like homeodomain transcription factor	0.24	0.38	5.6	1.6	23
	NAT19	*N*-acetyltransferase	0.43	1.4	8.5	3.3	20
	MYB16	Circadian clock–associated SWI/SNF complex	1.8	2.0	27	1.1	15
	Cre03.g172750	MYND finger	1.4	3.6	20	2.6	14
	HMG6	High mobility group protein	1.3	1.9	16	1.5	12
	NAT30	*N*-acetyltransferase	4.4	9.9	51	2.3	12
	Cre05.g248550	Hemerythrin HHE cation binding domain; CHY zinc finger	3.6	8.2	35	2.3	9.7
	MYB3	Myb-like transcription factor	4.7	5.0	28	1.1	6.0
	Cre07.g335150	Squamosa promoter binding protein	4.4	5.6	22	1.3	5.0
	NAT4	*N*-acetyltransferase	3.7	3.0	17	0.8	4.6
	Cre24.g770450	Basic helix-loop-helix family protein	32	53	109	1.7	3.4

Genes without functional annotation are indicated with the IDs corresponding to the version 4 assembly (Augustus 10.2). nd, not detected at the sequencing level used in this work. In such cases, fold changes were computed after imputation of missing values and should be understood as a lower bound of the actual value.

[a]Genes are sorted with respect to the fold changes in iron-limited conditions (0.25/20).

[b][Fe] in μM.

Table 2. Effect of Low Iron Nutrition on Tetrapyrrole Biosynthesis and Iron-Containing Proteins in Acetate-Grown Cells

			RPKM			Fold Change	
Process	Gene[a]	Defline	20[b]	1[b]	0.25[b]	1/20	0.25/20
Tetrapyrrole Biosynthesis	*FLP*	FLU chloroplast precursor	16	30	199	1.9	13
	HEM15	Ferrochelatase	23	40	129	1.7	5.6
	POR1	Protochlorophyllide reductase	64	47	243	0.7	3.8
	CHLI2	Magnesium chelatase subunit I	46	38	154	0.8	3.4
	GSA1	Glutamate-1-semialdehyde aminotransferase	36	23	119	0.6	3.3
	CPX1	Coproporphyrinogen III oxidase	40	29	128	0.7	3.2
	PBGD1	Porphobilinogen deaminase	32	20	101	0.6	3.1
	CHLI1	Magnesium chelatase subunit I	66	44	192	0.7	2.9
	GUN4	Tetrapyrrole binding protein	20	13	56	0.7	2.8
	GTS2	Glutamyl/glutaminyl-tRNA synthetase	32	23	86	0.7	2.7
	CHLD	Magnesium chelatase subunit D	32	19	87	0.6	2.7
	CLH1	Chlorophyllase I	2.2	2.4	6.0	1.1	2.7
	ALAD	δ-Aminolevulinic acid dehydratase	132	103	342	0.8	2.6
	CHLH1	Magnesium chelatase subunit H	63	62	159	1.0	2.5
	UROS	Uroporphyrinogen-III synthase	52	43	127	0.8	2.5
	UROD1	Uroporphyrinogen-III decarboxylase	49	26	106	0.5	2.2
	CHLG	Chlorophyll synthetase	37	26	79	0.7	2.1
Iron Proteins	*Cre09.g403550*	2OG-Fe(II)-dependent oxidoreductase	1.2	3.0	30	2.5	25
	Cre10.g427850	PAS fold	1.0	2.1	19	2.1	19
	CDJ3	Chloroplast DnaJ-like protein	19	45	300	2.4	16
	CDJ5	Chloroplast DnaJ-like protein	9.9	43	131	4.3	14
	FDX6	Ferredoxin 6	41	121	362	3.0	8.8
	FDX3	Ferredoxin 3	21	30	144	1.4	6.9
	BKT1	β-Carotene ketolase	1.7	1.5	9.3	0.9	5.5
	SOUL4	SOUL heme binding protein	4.3	4.6	21	1.1	4.9
	SOUL1	SOUL heme binding protein	34	55	133	1.6	3.9
	Cre10.g429750	PAS fold	2.8	3.1	10	1.1	3.6
	FXL1	FixL-like PAS domain protein	3.4	5.5	12	1.6	3.5
	ISC1	Iron-sulfur cluster assembly protein	31	50	91	1.6	2.9
	Cre10.g466700	2OG-Fe(II)-dependent oxygenase	6.2	8.4	18	1.4	2.9
	Cre13.g586600	Putative cytochrome b_{561} ferric reductase	4.8	5.5	16	1.1	3.3
	ACH1	Aconitate hydratase	1152	1162	566	1.0	0.5
	DES6	ω6-Fatty acid desaturase	1815	1807	892	1.0	0.5
	CYC	Mitochondrial cytochrome *c*	730	695	311	1.0	0.4
	FDX2	Ferredoxin 2	7.8	9.3	3.1	1.2	0.4
	MitoNEET	Iron sulfur domain-containing CDGSH-type subfamily	309	271	112	0.9	0.4
	CYP197-1	Cytochrome P450	28	28	9.8	1.0	0.4
	GSN1	Glutamate synthase, NADH-dependent	81	88	28	1.1	0.3
	Cre02.g093650	Rieske [2Fe-2S] domain-containing protein	421	356	127	0.8	0.3
	SIR1	Ferredoxin-sulfite reductase	121	83	20	0.7	0.2
	PHX5	Prolyl 4-hydroxylase	37	24	4.9	0.6	0.1

Genes without functional annotation are indicated with the IDs corresponding to the version 4 assembly (Augustus 10.2).
[a]Genes are sorted with respect to the fold changes in iron-limited conditions (0.25/20).
[b][Fe] in μM.

When we compared the sets of differentially expressed genes from acetate- versus CO_2-grown cells, we noted 214 genes in common in the iron limitation condition (Figure 3C, comparison A-C) and only 24 in common in the deficiency condition (Figure 3C, comparison B-D). Manual curation of the set of 24 (see Supplemental Data Set 3 online, sheet 3) indicates heavy representation of genes encoding the above-mentioned assimilatory and distributive transporters as well as components involved in stress response.

For the differentially regulated genes in iron-limited conditions, a greater proportion of downregulated genes was noted, perhaps reflecting the slower growth, which defines the limited state (Figures 4C and 4D). There are no major differences in how each functional class is represented in the two trophic conditions, although we did note that the category of respiration is not represented at all in the data set from CO_2-grown cells but includes a few downregulated genes in the data set from acetate-grown cells. Additionally, the category for photosynthesis

includes several downregulated genes encoding subunits of PSI and its associated antenna in the former data set.

Several genes required for biogenesis of iron-only hydrogenase (*HYDEF* and *HYDG*) or coding for iron-containing proteins like *PHX5* [encoding an Fe(II)-oxoglutarate dependent prolyl-4-hydroxylase], two hybrid-cluster proteins (*HCP1* and *HCP4*), and MitoNEET-like (Cre01.g050550), which possesses a CDGSH iron-sulfur domain and presumably binds a [2Fe-2S] cluster, are downregulated in iron-limited photoheterotrophic cells, perhaps as part of the iron-sparing response. By contrast, mRNAs for other iron-containing proteins, such as members of the cytochrome P450 family (*CYP744B1*, *CYP739A3*, and *CYP97C3*), cytochrome b_{561} (*Cre13.g586600*), or β-carotene ketolase (*BKT1*), increase. This may reflect the operation of a feedback mechanism geared toward ensuring the maintenance of these iron-containing proteins and is suggestive of a hierarchy of iron allocation to the many iron binding sites in the cell.

Taken together, functional analysis of genes regulated under iron-deficient and iron-limited conditions indicates changes in many iron-containing proteins and several transporters (a few, to our knowledge, not previously identified; Tables 1 and 2).

Iron Assimilation Components, Transporters, and Ferric-Chelate Reductases That Are Potentially Involved in Cellular Iron Distribution

The list of genes differentially expressed in iron deficiency (Figure 3A, comparisons B and D) was manually curated. In the first phase of the project, this involved improvement of the FM3.1 and FM4 models from the version 3 and 4 assemblies, respectively, and eventually the Augustus 5.1 and Augustus 10.2 models on the version 4 assembly, using coverage graphs to extend gene models, ESTs from 454 sequencing, and the paired-end reads to establish exon connectivity. In total, 73 gene models were improved, which in some cases allowed us to make functional assignments for a few uncharacterized loci.

Locus *Cre05.g248300.t1.1* is such an example (Figure 5A). In the original FM3.1 annotation (181027), this differentially expressed gene was represented by a small (703 bp) single exon gene without assigned function. The initial revision driven by the coverage graphs (genomes.mcdb.ucla.edu) revealed a multi-exon locus encoding an NRAMP transporter. This revision, incorporated into the most recent set of Augustus 10.2 annotations, *Cre05.g248300.t1.1*, is still slightly underpredicted because of a short gap in the genome sequence (chromosome_5:3,313,508-3,313,612) just after the 12th exon. Two 454 reads (SRR057479.655472 and SRR057479.939001) from the University of California-Los Angeles–Joint Genome Initiative (JGI) project (http://genomes.mcdb.ucla.edu/Cre454/) cover the gap, and the final revised sequence, now available at Phytozome (Cre05.g248300.t1.3, version 5.3 assembly), extends the 12th exon with 153 bp corresponding to 51 amino acid residues.

Sequence analysis of the NRAMP4 protein revealed that it contains nine transmembrane helices as predicted by the TMHMM algorithm (Sonnhammer et al., 1998) (see Supplemental Figure 3 online). A phylogenetic tree and similarity network of NRAMP transporters indicates that the *C. reinhardtii* NRAMP4 belongs to Eukaryotic Group I (Blaby-Haas and Merchant, 2012) and clusters with *Arabidopsis* NRAMP2, 3, 4, and 5 and with the mammalian counterparts (Figures 5B and 5C). It has been shown that *Arabidopsis NRAMP3* and *NRAMP4* are also induced in iron deficiency and both are targeted to the vacuole (Thomine et al., 2003; Lanquar et al., 2005). Since eukaryotic NRAMP proteins are involved in Fe^{2+} and/or Mn^{2+} transport, we used the pattern of expression as an indication of function. *NRAMP4* transcripts are ninefold induced in iron-deficient cells independent of carbon source, and this increases to 30- and 40-fold in iron-limited cells (Figures 6A and 6B). There are two other previously described NRAMP transporters encoded in the *C. reinhardtii* genome (*NRAMP1* and *NRAMP2*), and these are more likely to function in Mn^{2+} transport. Indeed, in contrast with NRAMP4, the tree and similarity network place NRAMP1 and NRAMP2 in the largely prokaryotic MntH Group B (Figures 5B and 5C). The expression of each *NRAMP* gene was evaluated in a separate experiment (Figure 6C). *NRAMP1* and *NRAMP2* transcripts are increased sixfold and twofold in manganese-starved cells, as previously observed (Allen et al., 2007b), while *NRAMP4* mRNA levels are elevated 19-fold after 12 h and eightfold after 24 h of iron starvation, respectively. Hence, we propose that NRAMP4 is involved in iron homeostasis, most likely localized to an internal compartment like its *Arabidopsis* ortholog (Lanquar et al., 2005).

Other potential components of intracellular iron distribution are TEF22 (Cre12.g546500), a ferric-reductase domain–containing protein (Cre05.g241400), a putative ferroportin (Cre16.g687000), and two proteins with homology to plant VIT1 and yeast Ccc1p (Cre02.g107550 and Cre02.g099500; Table 1). The *TEF22* transcript is more abundant in the presence of acetate compared with photoautotrophic cells (see Supplemental Data Set 5 online). *TEF22* is induced 7.6- and 17-fold in photoheterotrophic cells in response to iron deficiency and iron limitation, respectively, and in CO_2-grown cells even more dramatically, although the expression is always higher in acetate-grown cells. TEF22, located in the mitochondrion based on two proteomic studies (Allmer et al., 2006; Atteia et al., 2009), has a cytochrome b_{561} ferric-reductase domain at its C-terminal end (see Supplemental Figure 4 online). It is distinct from the classical cytochrome b_{561}–only containing proteins as TEF22 also contains a soluble heme binding DOMON domain in the central region. TEF22 is phylogenetically related to mammalian ferric-chelate reductases (FRSS1-like) and in protein similarity networks groups separately from Cre13.g586600, an ascorbate-dependent cytochrome b_{561} protein whose expression is increased 2.9-fold in iron limitation (see Supplemental Figure 5 online).

There are two homologs of *Saccharomyces cerevisiae* Ccc1p and *Arabidopsis* VIT1 (Table 1) (Li et al., 2001; Kim et al., 2006). These two proteins (Cre02.g107550 and Cre02.g099500) belong to a family of plant nodulin-like proteins, and their transcript abundances increase in response to poor iron nutrition (fivefold and twofold, respectively, under iron limitation; Table 1; see Supplemental Figure 6A online).

A previously undescribed putative ferric-reductase (Cre05.g241400) has increased transcript levels in response to poor iron nutrition under both photoheterotrophic and photoautotrophic conditions. This protein contains a conserved ferric-reductase–like

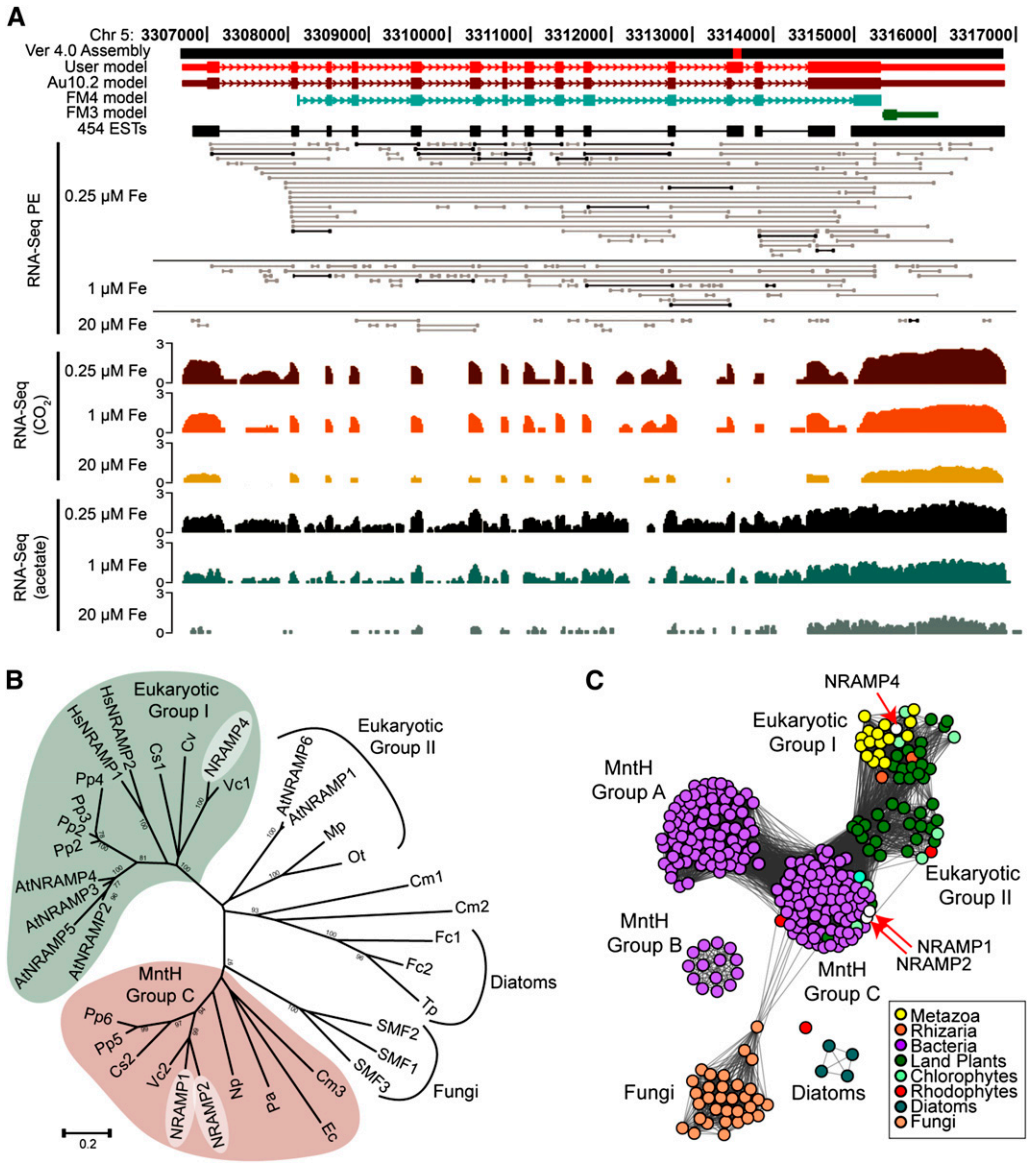

Figure 5. Identification of a New Protein of the NRAMP Transporter Family.

(A) Manual curation of the *NRAMP4* gene model. The figure shows a snapshot of the University of California, Santa Cruz browser and the JGI browser view of a gap present in the 4.0 version of the genome assembly (red square). JGI gene models, from version 3 (FM3) and version 4 (FM4) genome assembly, are in green and blue, respectively. The Augustus 5 gene model is in dark red and Augustus 10.2 in brown. The manually curated model, which used 454 ESTs to correct for the gap, is red (user model). Paired-end reads (RNA-Seq PE track), used to establish exon connectivity, are shown using different levels of gray to highlight the more frequent pairs (in black). The RNA-Seq coverage, on a $\log_{10}$ scale (shown to the left), from iron-limited (0.25 μM), iron-deficient (1 μM), and iron-replete (20 μM) cells grown under photoheterotrophic (acetate) and photoautotrophic (CO_2) conditions from one experiment is shown.
(B) Phylogenetic tree of NRAMPs homologs and orthologs from *C. reinhardtii* (NRAMP4, NRAMP1, and NRAMP2), *Arabidopsis* (At), *Physcomitrella patens* (Pp), *Homo sapiens* (Hs), *Coccomyxa subellipsoidea* C-169 (Cs), *Chlorella variabilis* NC64A (Cv), *Volvox carteri* f. *nagariensis* (Vc), *Ostreococcus tauri* (Ot), *Micromonas pusilla* CCMP1545 (Mp), *Escherichia coli* (Ec), *Nostoc punctiforme* (Np), *Pseudomonas aeruginosa* (Pa), *Fragilariopsis cylindrus* (Fc), *Thalassiosira pseudonana* (Tp), *Cyanidioschyzon merolae* (Cm), and *S. cerevisiae* (SMF1, SMF2, and SMF3).
(C) Protein similarity network of the NRAMP protein family. E-value cutoff for similarity was set at 1e-87.

transmembrane domain, an FAD binding domain, and a less conserved NAD binding domain near the C-terminal part (see Supplemental Figure 7 online). Ferric-reductase–like proteins are membrane proteins; indeed, Cre05.g241400 is predicted to possess nine transmembrane helices (see Supplemental Figure 7A online). The gene encoding this putative ferric-reductase (*Cre05.g241400*) is induced sixfold and ninefold in iron-deficient (1 μM iron) photoheterotrophically and photoautotrophically grown cells, respectively (see Supplemental Data Set 5 online). In iron limitation (0.25 μM iron), *Cre05.g241400* is significantly

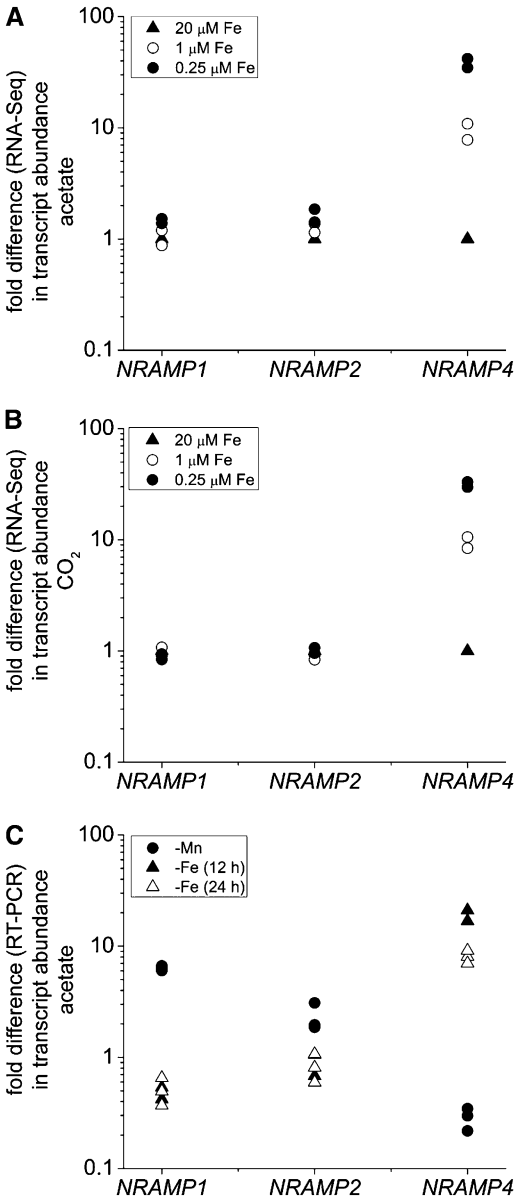

Figure 6. *NRAMP4* Transcript Abundance Is Increased Specifically in Response to Poor Iron Nutrition in *C. reinhardtii*.

(A) and **(B)** *NRAMP1*, *NRAMP2*, and *NRAMP4* transcript abundances estimated by RNA-Seq in *C. reinhardtii* cells grown under photoheterotrophic and photoautotrophic conditions and iron-replete, iron-deficient, and iron-limited conditions, respectively.

(C) Fold change of *NRAMP* transcripts assessed by real-time PCR in *C. reinhardtii* cells grown photoheterotrophically without manganese supplementation (circles) or without iron supplementation for the times indicated (triangles).

induced (14-fold and 20-fold in acetate- and CO_2-grown cells, respectively). *C. reinhardtii* Cre05.g241400 is more closely related to plant ferric-reductases than to the ferric-reductase protein family from yeast (see Supplemental Figure 7B online). Like TEF22, an ortholog of *Cre05.g241400* is present in *Volvox carteri*, but not in other algae with sequenced genomes (as of 6/2012). A protein similarity network (see Supplemental Figure 7C online) confirms that this putative *C. reinhardtii* ferric-reductase (Cre05.g241400) is similar to plant ferric-reductases and distinct from bacterial or fungal proteins. The protein similarity network additionally indicates a clear separation of ferric-reductases from the sequence-related respiratory burst oxidases and NADH-5 oxidases (see Supplemental Figure 7C online, inset). Like *TEF22*, *Cre05.g241400* is more dramatically upregulated in CO_2-grown cells, although it is always more highly expressed in acetate-grown cells.

A gene encoding a ferroportin-like protein (*Cre16.g687000*) is among the set of upregulated transcripts (Table 1). Based on the sequence similarity to ferroportin homologs, we modified the gene model using an upstream initiator Met, thus extending the protein by 58 amino acids. The curated gene model is available on the JGI browser (http://genome.jgi.doe.gov/cgi-bin/dispGeneModel?db=Chlre4&tid=536149). The protein contains two ferroportin (FPN1) domains, one in the N terminus and the second one in the C terminus; therefore, we name it FPN1. As expected, FPN1 is a membrane protein containing eight transmembrane helices, four in each FPN domain (see Supplemental Figure 8A online). Protein network similarity suggests that *C. reinhardtii* FPN1 is closely related to proteins in Streptophytes and Stramenopiles and is more distant from plant IREG3 proteins (see Supplemental Figures 8B and 8C online).

Together, the analysis indicates that under low iron nutrition, *C. reinhardtii* cells have increased transcript levels for two putative ferric-reductases (*TEF22* and *Cre05.g241400*). We propose that TEF22 and Cre05.g241400 might function together in reducing ferric iron to ferrous iron prior to its import into the mitochondria. There are two VIT1/CCC1 homologs and a ferroportin-like protein (FPN1), which we propose might function to transiently store iron in an intracellular compartment as it is mobilized by activation of iron-recycling mechanisms during poor iron availability in the growth medium.

Iron Limitation in *C. reinhardtii* Induces Nonenzymatic and Enzymatic Antioxidant Systems

Besides transporters, a second functional category represented in the data set includes several components of enzymatic and nonenzymatic antioxidant mechanisms. Most of these are induced in both photoautotrophic and photoheterotrophic cells, although the magnitude of the change and the basal level of expression in the replete situation may differ (e.g., see *MSD3* transcript abundance in Supplemental Data Sets 2 and 3 online). Genes encoding chloroplast ferritins (*FER1* and *FER2*), chloroplast manganese-superoxide oxidase (*MSD3*), and monodehydroascorbate reductase (*MDAR1*) are substantially upregulated (RPKM 10^2 to 10^3, fold changes from 6 to 10^3, depending on basal expression in the replete cells) (Table 1). These proteins can protect the cells from reactive oxygen species, which are expected to increase as a consequence of compromised function of PSI Fe/S centers in iron-starved cells. MnSOD3 is plastid localized and its upregulation in iron deficiency/limitation increases the capacity of the plastid to handle superoxide (generated in the Mehler reaction) without drawing on scarce intracellular iron (Page

et al., 2012). The increase in *FER* gene expression was also noted previously and was suggested to buffer chloroplast iron released by degradation of iron-containing proteins during iron salvage (Busch et al., 2008; Long et al., 2008). Chelation of iron would minimize the danger of iron reaction with hydrogen peroxide to generate hydroxyl radicals, which cannot be detoxified biochemically. The increase in *MDAR1* and *VITAMIN C 2* (*VTC2*) expression is a companion protective mechanism that detoxifies the hydrogen peroxide by increasing plastid ascorbate (Foyer and Noctor, 2011) (see below). Among enzymatic antioxidants, we noticed increased transcripts for glutaredoxin (*GRX6*), glutathione peroxidase (*GPX3*), thioredoxin-dependent peroxidase (*PRX6*), and a newly annotated peroxiredoxin (*Cre11.g471150*), but mainly only in the iron limitation stage when the cells are clearly stressed (Table 1).

Ascorbate is a well-known nonenzymatic antioxidant in the plant chloroplast (Gill and Tuteja, 2010; Foyer and Noctor, 2011). VTC2 catalyzes the committed step in de novo ascorbate biosynthesis in *C. reinhardtii* (Linster et al., 2007; Urzica et al., 2012), and MDAR1 catalyzes the conversion of monodehydroascorbate to ascorbate (Figure 7). This prompted us to validate the impact of changes in transcript abundance by measuring ascorbate content in iron-poor cells. Both photoautotrophically and photoheterotrophically grown cells have increased ascorbate content, in proportion with the increase in *VTC2* transcript abundance (Figures 7A and 7B). The increased ascorbate pool may require more recycling enzyme (MDAR1) to maintain the level of reduction. Quantitative proteomics and enzymatic assay of cell extracts confirmed the increase in the polypeptide and enzymatic activity, in each case approximately threefold and sixfold in iron deficiency and limitation (Table 3, Figure 7C). The increase in MDAR1 protein abundance is recapitulated at activity levels, as MDAR1 activity increased 3.6- and 6.3-fold under iron deficiency and iron limitation conditions, respectively.

In previous work, we noted an increase in the abundance of xanthophyll cycle pigments (although not nonphotochemical quenching) in iron-limited and iron-deficient cells with a more notable increase in photoheterotrophic conditions (Terauchi et al., 2010). Therefore, we surveyed genes encoding candidate enzymes of carotenoid metabolism in *C. reinhardtii* (Lohr et al., 2005, 2012) and Cre33.g783050, which was identified by BLAST search of the Augustus 10.2 annotation as an ortholog of *Arabidopsis* 15-*cis*-ζ-carotene isomerase. We noted increased mRNA abundances in acetate-grown cells but generally no changes or even reduced abundances in CO_2-grown cells (see Supplemental Data Set 6 and Supplemental Figure 9 online). We note that many of the enzymes, HDS, BKT1, CHYB, CYP97A5, and CYP97C3 are iron containing, and the increase in transcript abundance may reflect feedback regulation from loss of functional protein (see below). The absence of change in mRNAs for these genes in iron-deficient CO_2-grown cells might then indicate that those enzymes are resistant to loss of iron in photoautotrophic conditions.

Conservation of Iron Deficiency Responses between *C. reinhardtii* and Land Plants

In the past years, several genome-wide analyses were performed in iron-deficient plants (Colangelo and Guerinot, 2004; Dinneny et al., 2008; Buckhout et al., 2009; Zheng et al., 2009; Long et al., 2010; Yang et al., 2010). We wondered whether there might be conserved common responses to iron nutrition in the plant lineage. Therefore, we reviewed data sets from several such studies for orthologs of *C. reinhardtii* genes found in this work to be responsive to poor iron nutrition and found 14 proteins (Table 4). Among these are iron transporters like IRT1, IRT2, NRAMP4, VIT1-like, ferroportin, and a P-type ATPase homologous to *Arabidopsis* AHA2. In general, the pattern of regulation is similar (the transcripts are upregulated) with several exceptions. *NRAMP4* is downregulated in rice (Zheng et al., 2009), and the *VIT1*-like gene (*Cre02.g107550*) is downregulated in all *Arabidopsis* and rice transcriptome studies (Dinneny et al., 2008; Zheng et al., 2009; Long et al., 2010; Yang et al., 2010). *VIT1* expression is consistent with a function in long-term iron storage in seeds, whereas in a unicellular organism like *C. reinhardtii*, it is more likely to function in transitory storage during remobilization of iron from the chloroplast to the mitochondrion. The same is true for ferritins, which in *C. reinhardtii* are upregulated in deficiency, whereas in land plants they are downregulated (Briat et al., 1999; Busch et al., 2008; Dinneny et al., 2008; Long et al., 2008). MDAR1 is another globally conserved response, reflecting the importance of ascorbate as an antioxidant (Figure 7).

Of particular interest is Cre05.g248550, homologous to *Arabidopsis* BRUTUS (BTS). Cre05.g248550 contains four hemerythrin domains scattered throughout the length of the protein, a CHY-type zinc finger domain, and a putative E3 ubiquitin-protein ligase domain in the C-terminal part (see Supplemental Figure 10A online). Cre05.g248550 has homologs in land plants and other algae like *Chlorella* sp NC64A, *V. carteri*, *Ostreococcus* sp RCC809, and *Micromonas* spp (see Supplemental Figure 10B online). A protein similarity network clearly shows that Cre05.g248550 is closely related to *Arabidopsis* BTS and distinct from animal FBXL5 proteins, which are iron-sensing E3 ligases (Salahudeen et al., 2009; Vashisht et al., 2009) (see Supplemental Figure 10C online). We suggest that Cre05.g248550, which is induced in both photoautotrophic and photoheterotrophic cells, may be a functional ortholog of BTS.

Besides the proteins involved in iron homeostasis, there are a few proteins of unknown function: Cre10.g466050 and CGLD27 are pioneer proteins (i.e., they do not have domains suggestive of function), whereas Cre01.g061600 has a Kelch repeat and therefore may be part of a regulatory network. *CGLD27* encodes a highly conserved protein found in cyanobacteria and in all plastid-containing organisms, including diatoms (see Supplemental Figure 11 online). CGLD27 orthologs in *Arabidopsis* and rice are At5g67370 and Os03g0439700, respectively. The sequence contains a domain of unknown function (DUF1230), has three transmembrane segments, and is likely targeted to the chloroplast based on its relationship to open reading frame ycf36 encoded in some algal plastid genomes (Douglas and Penny, 1999).

In *Arabidopsis*, the CGLD27 ortholog is highly expressed in seeds, leaves, and flowers, whereas in roots its expression is the lowest (Figure 8A, left). The expression pattern is similar to that of *FRO3* encoding a ferric-reductase. Genes like *IRT1* (known to be involved in iron uptake in *Arabidopsis*) or *FC* (encoding ferrochelatase, an iron-using enzyme) have a different expression

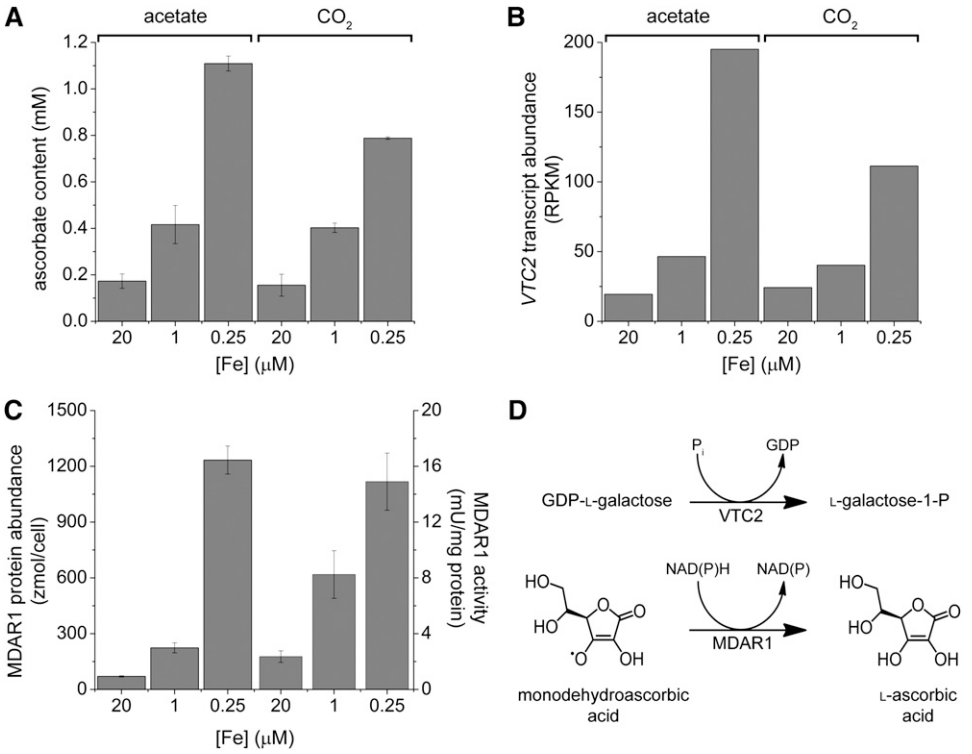

Figure 7. *C. reinhardtii* Cells Accumulate Vitamin C in Response to Low Iron Nutrition by de Novo Synthesis and Recycling.

C. reinhardtii cells were grown in iron-replete (20 μM iron), iron-deficient (1 μM iron), and iron-limited (0.25 μM iron) medium under photoheterotrophic (acetate) and photoautotrophic (CO_2) conditions.

(A) Vitamin C levels were measured by reversed-phase HPLC against a standard curve (Urzica et al., 2012). The identity of the peak was validated by its susceptibility to ascorbate oxidase.

(B) RNA-Seq analysis indicates an increase in the *VTC2* mRNA abundance under poor iron nutrition.

(C) Monodehydroascorbate reductase (MDAR1 encoded by *MDAR1*) activity and abundance is increased in response to iron deficiency. Extracts of soluble *C. reinhardtii* proteins from photoheterotrophically grown cells were analyzed for MDAR1 activity (right) and protein composition and abundance (left) by MS^E.

(D) The reactions catalyzed by VTC2 and MDAR1. Error bars indicate SD; $n = 3$.

pattern (Figure 8A, right). In a time-course experiment with root cells, *CGLD27* responds slightly more slowly than do *IRT1* and *FRO3*, which are highly upregulated under iron deficiency, reaching a maximum after 24 h of growing in iron-deprived conditions (Long et al., 2010). In *Arabidopsis*, *CGLD27* transcript levels increase progressively by 5-, 11-, and 12-fold after 24, 48, and 72 h of iron deficiency (Figure 8C).

We took advantage of a T-DNA insertional mutant with the insertion located in the second exon to test whether CGLD27 is required in iron-poor *Arabidopsis* plants. The mutant plants were grown under different iron concentrations: iron-replete conditions (100 μM iron) or iron-deficient (1 and 10 μM iron). In the presence of 10 to 100 μM iron, no visual phenotype could be observed between the wild type (Columbia-4 [Col-4]) and the *cgld27* mutant (Figure 8B). When the plants were grown in the presence of 1 μM iron, the *cgld27* mutant showed a stronger growth defect compared with Col-4. The mutant does not seem to be more chlorotic than Col-4 under iron-deficient conditions, but the root length is smaller in *cgld27* plants grown under 1 μM iron (Figure 8D). We also noted that plant fresh weight decreased when grown under iron deficiency, an effect that is stronger (twofold) for *cgld27* plants (Figure 8E). The phenotype is exacerbated in alkaline soil (pH 8.0) where the availability of iron is limited. Bayesian Markov Random Fields analysis (Kourmpetis et al., 2010) predicts a function for CGLD27/At5g67370 in carotenoid-xanthophyll metabolism. Moreover, *At5g67370* is coexpressed with *ZDS* (encoding ζ-carotene desaturase) in the ATTED-II database of coexpressed genes (Obayashi et al., 2007, 2011).

Together, these results validate the transcriptome analysis in *C. reinhardtii* cells grown under poor iron nutrition and show the importance of cross-species comparison.

Transcriptional Regulation of Iron Deficiency Responses

Where tested, most of the highly regulated genes (*FOX1*, *FTR1*, *FEA1*, and *MSD3*) are controlled at the transcriptional level (Allen et al., 2007a; Page et al., 2012). Deletion analysis identified candidate iron response elements (FeREs) in the 5′ flanking regions of the *FOX1*, *FTR1*, *FEA1*, and *ATX1* genes (Deng and Eriksson, 2007; Fei and Deng, 2007; Fei et al., 2009, 2010). Two distinctive *cis*-acting elements were identified: CAC(G/A)CG in the promoter regions of *FOX1*, *FEA2*, or *FER1* and TG(G/C)CA in the promoters

Table 3. Changes in Abundances of Antioxidant and Iron-Containing Proteins in Photoheterotrophic Cells

Gene Name	Defline	Bound Fe Species	Protein Abundance (μmol/Cell)			Fold Change			Direction of Regulation	
			20 μM Iron	1 μM Iron	0.25 μM Iron	1/20	0.25/20	0.25/1	Protein	mRNA[a]
Antioxidants										
MSD3	Mn superoxide dismutase		nd	10 ± 3	73 ± 21	na	na	7	↑	↑
MDAR1	Monodehydroascorbate reductase		70 ± 4	224 ± 27	1234 ± 75	3	18	6	↑	↑
GRX6	Glutaredoxin, CGFS type		nd	6 ± 5	18 ± 6	na	na	3	↑	↑
GSH1	Glutathione synthetase		34 ± 0.7	45 ± 11	95 ± 19	1	3	2	↑	↑
NRX2	Nucleoredoxin 2		8 ± 6	nd	26 ± 5	na	3	na	↑	↑
FER1	Ferritin	Fe^{2+}	23 ± 2	68 ± 15	53 ± 11	3	2	1	↑	↑
TRXH	Thioredoxin		13 ± 0.6	17 ± 10	30 ± 6	1	2	2	↑	=
GSTS3	Glutathione *S*-transferase		13 ± 13	37 ± 22	nd	3	na	na	↑	=
CCPR1	L-ascorbate peroxidase, heme-containing	Heme	5 ± 3	nd	16 ± 4	na	3	na	↑	↓
Iron-Containing Proteins										
FEA2	Iron-assimilating protein	Fe^{3+}	nd	97 ± 16	512 ± 77	na	na	5	↑	↑
FEA1	Iron-assimilating protein	Fe^{3+}	124 ± 21	735 ± 34	1356 ± 115	6	11	2	↑	↑
SOUL1	SOUL heme binding protein	Heme	6 ± 0.3	10 ± 5	23 ± 2	2	4	2	↑	↑
TEF22	Predicted protein	Heme	nd	nd	41 ± 26	na	na	na	↑	↑
RIR2A	Ribonucleotide reductase R2 subunit	Di-iron	nd	10 ± 0.7	11 ± 0.8	na	na	1	↑	↑
ADH1	Alcohol/acetaldehyde dehydrogenase	Fe^{2+}	6 ± 1	12 ± 6	33 ± 10	2	6	2	↑	=
FSD1	Iron superoxide dismutase	Fe^{2+}	340 ± 42	300 ± 48	320 ± 87	1	1	1	=	=
CYC	Mitochondrial cytochrome *c*	Heme	83 ± 14	66 ± 7	71 ± 11	1	1	1	=	↓
ACH1	Aconitatehydratase	[4Fe-4S]	379 ± 25	408 ± 69	280 ± 35	1	1	1	=	↓
FAB2	Plastid acyl-ACP desaturase	Di-iron	47 ± 19	56 ± 16	23 ± 9	1	0.5	0.4	↓	↑
GSF1	Ferredoxin-dependent Glu synthase	[3Fe-4S]	108 ± 8	91 ± 3	43 ± 7	1	0.4	1	↓	↑
HDS1	4-Hydroxy-3-methylbut-2-en-1-yl diphosphate synthase	[4Fe-4S]	125 ± 37	95 ± 4	23 ± 7	1	0.2	0.2	↓	↑
FRR2	Ferredoxin thioredoxin reductase	[4Fe-4S]	18 ± 2	14 ± 1	6 ± 2	1	0.4	0.4	↓	=
LEU1L	Isopropylmalate dehydratase, large subunit	[4Fe-4S]	159 ± 18	151 ± 25	54 ± 1	1	0.3	0.4	↓	=
APR	Adenylylphosphosulfate reductase	[4Fe-4S]	129 ± 26	104 ± 3	43 ± 10	1	0.3	0.4	↓	=
GSN1	Glu synthase, NADH-dependent	2x[4Fe-4S]; [3Fe-4S]	46 ± 10	32 ± 10	13 ± 2	1	0.3	0.4	↓	↓
01.g050550	CDGSH Fe/S domain-containing protein	[2Fe-2S]	37 ± 6	26 ± 6	nd	1	na	na	↓	↓
HCP3	Hybrid-cluster protein	[4Fe-2S-2O]; [4Fe-4S]	11 ± 6	3 ± 0.4	nd	0.3	na	na	↓	↓
PETF	Ferredoxin	[2Fe-2S]	87 ± 35	30 ± 27	nd	0.3	na	na	↓	↓

Proteins were identified and quantified based on the signal intensity of the three most abundant peptides by MS^E (Castruita et al., 2011). Values represent the averages of three biological replicates; SD is indicated. The up arrow indicates increases in RNA or protein abundance in iron-deficient or -limited cells, a down arrow indicates decreases, and an equals sign indicates that there is no change. The presence of bound Fe(II/III) species was inferred from sequence alignments and the conservation of Fe(II/III) coordinating residues in previously characterized members of those protein families from other organisms. The complete list of proteins identified and quantified by mass spectrometry (Elevated Energy) (MS^E) is available in Supplemental Data Set 7 online.

[a]Changes in mRNA abundances as analyzed by RNA-Seq. na, not applicable. nd, not detected.

of *FEA1*, *FRE1*, and *ATX1*. To determine the relevance of these elements to the differentially expressed genes identified in this work, we searched the 5′ flanking regions after using the coverage graphs to adjust gene models to reflect the 5′ most end of each transcript (the presumed transcription start site). An unsupervised promoter analysis (Castruita et al., 2011) on different iron deficiency gene sets (Figure 3A, comparisons A-B, C-D, and B-D) shows that for short promoters (<1000 bp upstream of the transcription start site), CACGCG is the most overrepresented 6mer, both for photoheterotrophic and photoautotrophic conditions (see Supplemental Figure 12 online). The same analysis failed to find significant overrepresentation for motifs of the type TG(G/C)CA. Moreover, no significant results were found for longer words (7-8mers), indicating that the core sequence for FeREs of the type CAC(G/A)CG is restricted to these six nucleotides (see Supplemental Figure 12 online). We conclude that CAC(G/A)CG is likely to be a fundamental component of iron signaling, while TC(G/C)CA may

Table 4. Conservation of Responses to Iron Nutrition between *C. reinhardtii* and Land Plants

		This Study	b	c	d	e	f	g
		Transcript Regulation						
Protein Name[a]	Defline	*C. reinhardtii*	*Arabidopsis*					Rice
IRT1[b]	Iron nutrition–responsive ZIP family transporter	↑	+	+	+	+	+	+
NRAMP4	Putative Mn/metal transporter, NRAMP homolog	↑	+	+	+	+	+	−
IRT2[b]	Iron nutrition–responsive ZIP family transporter	↑	+	+	+	+	+	+
Cre10.g466050	Expressed hypothetical protein	↑		+		+	+	+
Cre01.g061600	Kelch repeat protein	↑	+	+	+	+	+	+
MDAR1	Monodehydroascorbate reductase	↑		+		+		+
Cre14.g609500	Expressed hypothetical protein	↑			+			
FER1[b]	Ferritin	↑		−	−		−	−
Cre16.g687000[b]	Similar to ferroportin	↑	+		+	+	+	+
CGLD27	Expressed hypothetical protein	↑		+	+	+	+	+
CDJ3	Chloroplast DnaJ-like protein	↑		+	+	+		+
Cre05.g248550[b]	Hemerythrin binding domain; CHY zinc finger, E3 ligase	↑		+	+	+	+	+
Cre02.g107550	VIT1 family	↑		−	−		−	−
PMA2[b]	P-type ATPase/cation transporter	↑	+	+			+	

Up arrow indicates an increase in expression in low iron relative to the replete situation. A plus sign indicates that a gene encoding an ortholog (or homolog) in *Arabidopsis* or rice is similarly regulated, a minus sign indicates opposite regulation, and a blank means that no information is available in the cited study. The data for *Arabidopsis* and rice were manually curated from (b) Colangelo and Guerinot (2004), (c) Dinneny et al. (2008), (d) Long et al. (2010), (e) Buckhout et al. (2009), (f) Yang et al. (2010), and (g) Zheng et al. (2009).

[a]*C. reinhardtii* protein name and defline (protein description) is indicated.

[b]Identification of orthologs by mutual best hit is often precluded for members of multigene families.

regulate only a subset of genes through a parallel signal transduction pathway.

Besides the FeREs, little else is known about the regulation of iron-deficient responses in *C. reinhardtii*. Among the differentially expressed genes is *Cre24.g770450* (see Supplemental Figure 13A online). Its expression is two- to threefold increased in iron-poor conditions in both CO_2- and acetate-grown cells (Table 1). The *C. reinhardtii* protein is similar to the *Arabidopsis* group IV transcription factors (ILR3, bHLH34, bHLH104, and bHLH115) (see Supplemental Figure 13B online). In *Arabidopsis*, at least two basic helix-loop-helix (bHLH) transcription factors are involved in signaling iron deficiency responses, FIT1 and PYE. *FIT1* expression is increased in iron-deficient roots, and the protein interacts with other bHLH factors (bHLH38 and bHLH39), forming a heterodimer that regulates *FRE1* and *IRT1* expression (Colangelo and Guerinot, 2004; Jakoby et al., 2004; Yuan et al., 2005, 2008). PYE interacts with the bHLH transcription factor ILR3, which itself interacts with BTS (discussed above) (Rampey et al., 2006; Long et al., 2010). Both *PYE* and *BTS* are upregulated in iron-deficient *Arabidopsis*. We hypothesize that the *C. reinhardtii* bHLH Cre24.g770450 protein might be an entry to identification of the network of transcriptional regulators that influence iron deficiency responses in algae.

Several other transcription factors are induced at the transcript level under iron-deficient and -limited conditions (Table 1). Among them, we identified three Myb-like transcription factors (*MYB4*, *MYB16*, and *Cre12.g514400*). Myb-like transcription factors have been previously associated with iron deficiency in plants, where they might function as regulators of iron deficiency responses (Chen et al., 2006; Ogo et al., 2006; Shen et al., 2008) or they are involved in senescence (Sperotto et al., 2008). Additionally, three genes coding for GCN5-related *N*-acetyltransferases (*NAT19*, *NAT30*, and *NAT4*) were strongly upregulated (Table 1). Several GNAT-like proteins were found to be induced in *Arabidopsis* in response to iron deficiency (Dinneny et al., 2008; Schuler et al., 2011). GCN5-related acetyltransferases are involved in histone acetylation and usually associated with the activation of gene transcription. Thus, at least in *Arabidopsis* and *C. reinhardtii*, iron limitation may result in enhanced histone acetylation that might be necessary to make chromosomal areas more accessible for transcriptional machineries.

Quantitative Analysis of the Soluble Proteome from Photoheterotrophically Grown *C. reinhardtii* Cells

To assess whether the changes in the transcriptome from iron-deficient and iron-limited cells are recapitulated at the protein level, we performed quantitative proteomics on the soluble proteome of the photoheterotrophic *C. reinhardtii* cells. After fractionation of total soluble proteins by gel electrophoresis and trypsin digestion of the fractions, we identified and quantified peptides derived from each fraction by liquid chromatography–tandem mass spectrometry. Data were searched against the Augustus 10.2 gene models (Phytozome). As many as 992 proteins were identified, of which 524 were reliably quantified (S.I. Hsieh, M. Castruita, D. Malasarn, E.I. Urzica, J. Erde, M.D. Page, D. Casero, M. Pellegrini, S.S. Merchant, and J.A. Loo, unpublished data). A subset of 53 proteins, relevant to this study, is presented here (see Supplemental Data Set 7 online).

The differentially expressed proteins can be divided into three groups. In one group are proteins whose changes in abundance

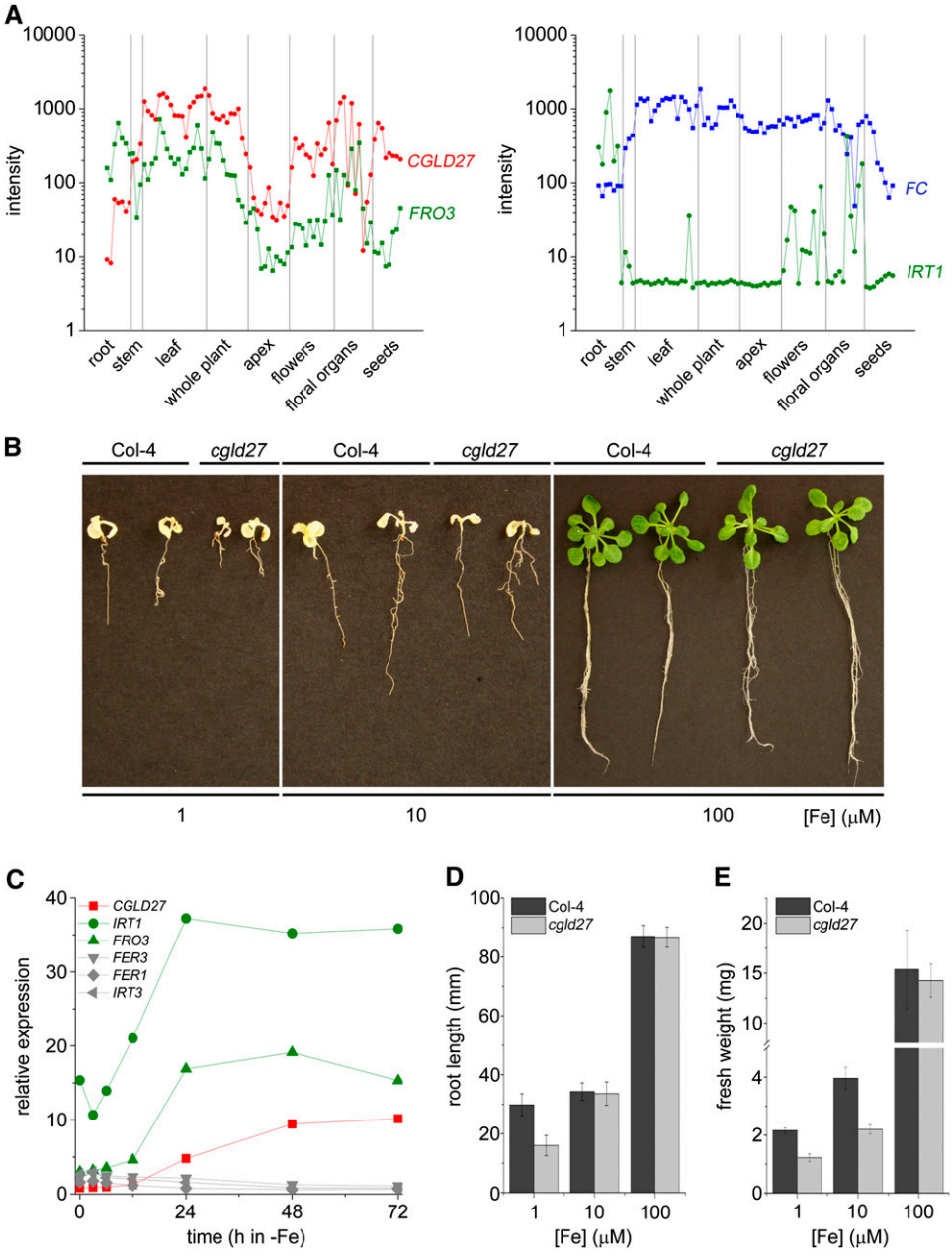

Figure 8. *Arabidopsis cgld27* Shows Increased Sensitivity to Poor Iron Nutrition.

(A) Pattern of expression of *CGLD27*, *FRO3*, *IRT1*, and ferrochelatase (*FC*) in *Arabidopsis* organs. Signal intensities for these genes were extracted from AtGenExpress developmental microarrays (Schmid et al., 2005).

(B) Phenotype of *Arabidopsis* wild type (Col-4) and *cgld27* mutant were grown in iron-replete (100 μM iron) and iron-deficient conditions (1 and 10 μM iron) for 2 weeks.

(C) Relative abundances of *CGLD27*, *IRT1*, *IRT3*, *FRO3*, *FER1*, and *FER3* transcripts in response to iron starvation in *Arabidopsis*. Data are from Long et al. (2010).

(D) Root length of wild-type and *cgld27* plants grown in the presence of 100, 10, and 1 μM iron (error bars indicate SD; $n = 10$).

(E) Fresh weight of wild-type and *cgld27* plants grown in different iron concentrations (SD is indicated; $n = 5$).

(16 increased and seven decreased) match the changes observed for transcript abundance (Table 3). Among the ones that increase are iron assimilation proteins, FEAs and TEF22, antioxidant or stress response proteins, MnSOD3, monodehydroascorbate reductase, ferritin1 and GSH1, and, interestingly, ribonucleotide reductase, which is a highly prioritized iron-containing protein because of its role in DNA synthesis. By contrast, the proteins that decrease with corresponding decreases in mRNAs tend to contain bound iron. This includes many Fe/S cluster proteins, such as Cre01.g050550, HCP3, and ferredoxin. The coordinate

decrease of both protein and RNA abundance suggests that these are downregulated as primary targets in an iron-sparing program. Several proteases, SCPL50, CEP1, and MMP13, are also increased in conjunction with their RNAs (Table 3; see Supplemental Data Set 7 online), perhaps implicating them in the degradative activities involved in iron recycling and photoprotection (Moseley et al., 2002; Page et al., 2012).

In a second group are proteins that are reduced in abundance without an effect on mRNA abundance. In this group are many Fe/S proteins (Table 3). It is possible that the protein levels cannot be maintained because of reduced iron supply for Fe/S biogenesis or that photooxidative stress results in damage of these proteins, leading to their eventual degradation. Finally, there is a third group, where changes in protein are opposite to those noted for the RNAs. Again, many (e.g., ADH1, FAB2, and GSF1), although not all (e.g., RPE1, PBGD1, UROD1, LCIC, and LCIB), of these are iron-containing proteins. For these, we suspect that increased RNA abundance is a secondary rather than direct effect of iron deficiency physiology: low protein abundance having a feedback effect on raising transcript levels. In fact, most of the Fe/S cluster–containing proteins identified in the proteomic analysis (Table 3; see Supplemental Data Set 7 online) are reduced in abundance in iron-limited cells, independent of their mRNA abundances, pointing to the impact of poor iron nutrition on Fe/S proteins.

Although we used only soluble fractions (supernatant from 253,000*g* centrifugation), we did identify peptides from membrane proteins (FOX1 and TEF22), indicative perhaps of some degradation in the extramembrane domains. Therefore, the abundance of these proteins is underestimated. Since the ferroxidase could not be detected in the proteome from iron-replete cultures, a fold change could not be calculated. Nevertheless, the change in *FOX1* mRNA abundance is approximately comparable to the change in protein abundance estimated from immunoblots (Figure 2; La Fontaine et al., 2002).

Photoautotrophic versus Photoheterotrophic

There are substantial differences in the transcriptomes of photoautotrophic versus photoheterotrophic cells independent of iron nutrition. To focus attention on quantitatively meaningful changes, we applied a stringent cutoff fold change of $\geq$8 (FDR<5%). Samples were compared pairwise with carbon source as the variable (see Supplemental Figure 1, comparisons E to G, and Supplemental Data Set 4 online). The combination of (1) the stringent cutoff and (2) the different impact of iron deficiency on trophic status reduced the number of genes that are always differently expressed in CO_2 versus acetate (intersection of comparisons E, F, and G) to only 114. These dramatically regulated genes are largely associated with carbon source utilization. In CO_2-grown cells, the carbon concentrating mechanism is induced, while in acetate-grown cells, genes encoding enzymes involved in acetate utilization are induced. Of nine carbonic anhydrases, three contribute significantly to the *CAH* mRNA population, *CAH1*, *CAH4*, and *CAH5*, with abundances corresponding to 2332, 2184, and 1180 RPKM in iron-replete cultures, respectively. The mRNAs are maintained in iron-deficient and -limited cells, consistent with the operation of photosynthesis, whereas in acetate-grown cells, their low level of expression is further repressed. Interestingly, there are a few genes in this list representing uncharacterized proteins (e.g., Cre11.g477350, Cre59.g791750, Cre12.g554100, Cre01.g003950, Cre18.g748750, Cre10.g457194, Cre02.g073600, and Cre02.g120200) that we suspect, based on their pattern of expression, are likely to be involved in the carbon concentrating mechanism. A recent study (Fang et al., 2012) has suggested a potential function as C_i transporters for some of these proteins (e.g., Cre11.g477350, Cre59.g791750, Cre12.g554100, and Cre01.g00395). The gamma carbonic anhydrases are more highly expressed in acetate-grown cells, consistent with their function in mitochondrial respiration (Cardol et al., 2004, 2005).

The data set also gives an opportunity to compare the expression of individual members of gene families (see Supplemental Data Set 8 online). For instance, *FBA3* with an expression level corresponding to $\sim 3 \times 10^3$ RPKM is the most highly expressed fructose-1,6-bisphosphatase–encoding gene. Iron nutrition does not affect its abundance but does affect expression of a different isoform, *FBA1*, in acetate-grown but not in CO_2-grown cells. Other examples include *ACS3* versus *ACS1* and *ACS2*, *PGK1* versus *PGK2*, and *RBCS2* versus *RBCS1*. *RBCS2* is regulated by carbon source, with an expression level of 3×10^4 RPKM in CO_2-grown cells or approximately three- to fourfold greater than the level in acetate-grown cells.

DISCUSSION

In this study, we used RNA sequencing methods to reveal genes whose expression is affected by poor iron nutrition. In previous work, we identified components of iron assimilation (e.g., FEA1, FRE1, FOX1, and FTR1) in *C. reinhardtii* and noted (1) that the genes were transcriptionally regulated by iron and (2) that the increase in transcript abundance occurred when the iron content of the medium was marginally deficient, without an impact on chlorophyll content, photosynthesis, or growth rate. This suggested that a comparative transcriptome would be a fruitful approach to the identification of other target genes of nutritional iron signaling and further that genes that are upregulated in asymptomatic iron-deficient cells might represent direct targets of iron signaling (as expected for components of iron assimilation) rather than secondary consequences of stress resulting from loss of function of iron proteins.

C. reinhardtii cells have two lifestyles: autotrophic growth on CO_2 and heterotrophic growth on acetate. In either case, metabolism depends on abundant iron proteins, the former on proteins of the photosynthetic apparatus in the chloroplast and the latter on mitochondrial respiratory complex proteins. We analyzed iron deficiency responses in both conditions to distinguish compartment- or pathway-specific processes and the occurrence of iron-sparing mechanisms that might control iron supply to mitochondria versus chloroplasts. The experiments also allowed us to compare the transcriptomes of acetate versus CO_2-grown cells (Figure 3; see Supplemental Figure 1 and Supplemental Data Set 4 online). The expression estimates between independent experimental replicate samples are exceptionally similar over three orders of magnitude, as noted in previous studies (Castruita et al., 2011).

Interaction between C Source and Iron Nutrition

Similar numbers of genes are differently expressed in acetate- versus CO_2-grown cells independent of iron supply (see Supplemental Figure 1 and Supplemental Data Set 4 online). In iron-replete medium, 3 to 4 $\times$ 10^3 genes are differentially expressed if we use a twofold cutoff and $\sim$1 $\times$ 10^3 with a fourfold cutoff (FDR <1%). In all cases, more genes are differentially expressed in iron-replete medium and the least in iron-limited medium. To focus the analysis on genes that showed significant fold change, we arbitrarily chose a cutoff of eightfold for presentation in this article, which yielded between 2 and 3 $\times$ 10^2 genes in each list and only 114 common among the three comparisons. This is because the expression of some of the genes is influenced by both carbon source and iron nutrition (e.g., *LHCBM7* and *MSD3*), and in some comparisons the difference in expression does not reach the stringent eightfold cutoff. In other cases, the impact of iron nutrition is dependent on the mode of growth (autotrophic versus heterotrophic), as noted previously (Naumann et al., 2007; Terauchi et al., 2010). Genes in this category include *DES6*, *Cre01.g056250* encoding a pioneer protein, and *CGLD27*, among others. Previous studies indicate that photoautotrophic cells are more effective at maintaining their iron quota, which means that given the same supply of iron in the medium, the gene regulation pathways may not be as highly activated in CO_2-grown cells versus the acetate-grown ones.

Besides some components of the CCM (like *CAH* and *LCI* genes, which are documented to increase in cells grown at air levels of CO_2; Yamano and Fukuzawa, 2009; Wang et al., 2011), the core list of 114 genes contains a number of known or candidate regulatory proteins (LCR1, CDKG2, PPP30, HOR1, and SNF2-like) or possibly biogenesis/assembly factors (DNJ15, DNJ31, MRPS17, and ribosomal proteins), reflecting the proliferation of mitochondrial versus chloroplast machinery in acetate- versus CO_2-grown cells. The fact that there are several pioneer proteins in this list indicates considerable room for new discovery in understanding carbon metabolism in green algae. For instance, we note that a long-chain acyl-CoA ligase and a triacylglycerol lipase are more highly expressed in CO_2- versus acetate-grown cells, suggesting that in the former situation, (activated) acetate may likely be generated by triacylglycerol and fatty acid degradation.

Tetrapyrrole Metabolism

One of the classic and diagnostic symptoms of iron deficiency is chlorosis, attributed to inhibition of chlorophyll biosynthesis (e.g., via reduced function of the di-iron cyclase but also via an effect on ferrochelatase for heme biosynthesis) and programmed degradation of chlorophyll-protein complexes (Spiller et al., 1982; Moseley et al., 2002; Yadavalli et al., 2012). Acetate-grown cells have reduced chlorophyll content under iron limitation, but photoautotrophic cells are less affected (Figure 1). Curiously, in acetate-grown cells, nearly all transcripts of the tetrapyrrole biosynthetic pathway (heme and chlorophyll branches) are increased in iron limitation, whereas in photoautotrophic cells, they are decreased (see Supplemental Figure 14 and Supplemental Data Set 9 online), suggesting that mRNA abundance is sensitive to feedback inhibition from the end products. Indeed, *FLP1* and *GUN4* (potential regulators of tetrapyrrole biosynthesis) are dramatically changed. *FLP1* is induced 1.9- and 13-fold in response to iron deficiency and iron limitation, respectively (see Supplemental Data Set 9 online).

Conserved Responses to Poor Iron Nutrition

Only 24 genes are differently expressed in mildly iron-deficient cells independent of lifestyle, and they tend to encode iron transporters and associated functions or stress response proteins, particularly antioxidants (Table 1). We suggest that these are primary and direct targets of nutritional iron signaling, which is supported by the enrichment of candidate FeREs in the 5′ upstream sequences flanking the start site of transcription (see Supplemental Figure 12 online). When we compared the responses in *C. reinhardtii* to those documented in *Arabidopsis*, tomato (*Solanum lycopersicum*), and rice, transporters and antioxidant proteins were well represented as well, indicative of the importance of these processes throughout the plant lineage. In fact, several studies have demonstrated that iron deficiency results in enhanced antioxidant mechanisms in plants, algae, and diatoms (Zaharieva and Abadía, 2003; Allen et al., 2008; Li et al., 2008; Thamatrakoln et al., 2012).

Ascorbate appears to be a key defense response. In *C. reinhardtii*, this occurs by upregulation of de novo ascorbate synthesis via VTC2 as well as by recycling via MDAR1 (Figure 7D). We showed that increased *MDAR1* transcript abundance results directly in increased protein and enzyme activity and contributes to the as much as 10-fold increased abundance in ascorbate content.

Other conserved responses include some uncharacterized proteins, such as CGLD27, Cre10.g466050, Cre01.g061600, and Cre14.g609500, and homologs of *Arabidopsis* BTS, an E3 ligase with an iron binding site that is known to be involved in regulation of iron homeostasis (Table 4). The fact that these responses are conserved over a billion years of evolution underscores their importance and relevance and suggests that reverse genetic analysis of these uncharacterized proteins could be especially rewarding for deeper understanding of the cell biology of nutritional iron homeostasis. Since CGLD27 is conserved also in cyanobacteria and diatoms, but is not present in the genomes of nonphotosynthetic organisms (Karpowicz et al., 2011), we tested its relevance in *Arabidopsis* and found that *cgld27* plants displayed an aggravated iron starvation phenotype, consistent with a function in iron homeostasis (Figure 8). Although CGLD27 is likely localized to plastid membranes, it is expressed in roots; therefore, it is unlikely to function directly in photosynthesis. Rather, it must have a role in some other fundamental metabolic pathway that is dependent on iron.

In two cases, the direction of regulation in *C. reinhardtii* versus a higher plant is opposite. This might be a consequence of the different functions of cells in a multicellular organism with specialized organs. For instance, the root is specialized for iron uptake from the soil, while the green organs are sinks for iron utilization. Ferritin is one example of this, where it is increased in high iron conditions in plant roots to buffer and detoxify excess

assimilated iron, whereas in *C. reinhardtii* chloroplasts, it has a role in transient buffering of iron as it is released from the degradation of chloroplast iron proteins en route to the mitochondrion (Briat and Lobréaux, 1997; Busch et al., 2008).

A comparison of iron deficiency transcriptomes of five *Arabidopsis* ecotypes identified a small set of 10 upregulated genes in all ecotypes or 24 upregulated genes in four out of five ecotypes out of hundreds or more than a thousand differentially regulated genes within an ecotype (Stein and Waters, 2012). There is a striking overlap between this set of 10 core/24 common genes from the *Arabidopsis* ecotype study and the 14 genes identified in this contribution. Interestingly, ferritin, classically used as an indicator of iron status, is not upregulated, at least at the transcript level, in all *Arabidopsis* ecotypes.

Iron Assimilation: Transporters and Ferrireductases

Because of the importance of iron as a nutrient, most organisms have multiple pathways for assimilating iron from various chemical forms (ferrous versus ferric and chelated versus insoluble oxides). Previously, we identified a number of iron assimilation components, FRE1, FOX1, FTR1, FEAs, and IRTs (Figure 9), in *C. reinhardtii* based on homology to those in yeast, animals, and *Arabidopsis* (Philpott, 2006; Jeong and Guerinot, 2009). We suggest that some of the newly identified targets are probably also involved in iron transport (Table 1). For instance, we hypothesize that *C. reinhardtii* PMA2, orthologous to *Arabidopsis* AHA7 and with high sequence similarity to *Arabidopsis* AHA2, might have a role in medium acidification to solubilize Fe(III). Both *Arabidopsis* genes (*AHA2* and *AHA7*) are induced in response to iron deficiency (Colangelo and Guerinot, 2004; Dinneny et al., 2008; Santi and Schmidt, 2009; Yang et al., 2010). AHA2 is responsible for rhizosphere acidification, whereas AHA7 is required for the formation of iron-induced root hairs (Santi and Schmidt, 2009).

Two genes, *Cre01.g010400* and *Cre13.g588700*, encode *C. reinhardtii* proteins of unknown function. The change in expression noted in this work is consistent with the increased abundance of the corresponding proteins in an earlier independent proteomic study of plasma membrane proteins from iron-deficient *C. reinhardtii* cells (Reinhardt et al., 2006). We hypothesize that Cre01.g010400 and Cre13.g588700 may be components in a novel iron assimilation pathway (like the FEAs), or, based on their location in the plasma membrane, they might play a role in sensing extracellular iron supply.

Once inside the cell, iron has to be distributed to different intracellular compartments where it is needed in essential iron-containing proteins (chloroplast and mitochondrial electron transfer chains) (Figure 9). Iron-deficient *C. reinhardtii* cells upregulate several genes encoding transporters with the potential to function in intracellular metal distribution. These include *NRAMP4*, *Cre16.g687000* encoding ferroportin, *Cre02.g107550* encoding a CCC1-like transporter, and *ATM3* (Figure 9).

The NRAMP proteins are conserved from bacteria to humans. They catalyze the H^+-dependent transport of divalent metal ions, such as Mn^{2+}, Fe^{2+}, Co^{2+}, Zn^{2+}, Ni^{2+}, or Cd^{2+} (Courville et al., 2006; Nevo and Nelson, 2006). The yeast genome codes for three NRAMP transporters (Sm1p, Smf2p, and Smf3p), of which Smf3p is vacuolar membrane localized and its expression is regulated by iron nutrition, whereas mammals have two, SLC11A1 and SLC11A2 (Portnoy et al., 2000; Singh et al., 2007). The *C. reinhardtii* genome codes for three NRAMPs (NRAMP1, NRAMP2, and NRAMP4). Mammalian SCL11A2 (also called DCT1/DMT1) functions in iron import into enterocytes, after reduction of ferric iron by ferric-reductase at the apical membrane, and in Fe^{2+} transport from the endosome during the transferrin cycle (Riedel et al., 1995; Andrews, 2000). *NRAMP3* and *NRAMP4* in *Arabidopsis* are both induced by iron deficiency (Thomine et al., 2000) and function to mobilize iron from vacuoles during seed germination (Lanquar et al., 2005). *C. reinhardtii NRAMP4* is induced by iron deficiency under both photoheterotrophic and photoautotrophic conditions. Changes in *NRAMP4* mRNA abundances are specific to iron-deficient cells, whereas the *NRAMP1* and *NRAMP2* genes are induced specifically in manganese-starved cells. Bioinformatic analyses revealed that NRAMP4 from *C. reinhardtii* is more closely related to *Arabidopsis* NRAMP3/4 and mammalian DCT1 than to the other *C. reinhardtii* NRAMP proteins. Therefore, we hypothesize that *C. reinhardtii* NRAMP4 is involved in remobilization of vacuolar iron stores needed for essential processes (photosynthesis and mitochondrial respiration) during low iron nutrition. A compartment called the acidocalcisome has been described in *C. reinhardtii* (Ruiz et al., 2001). This compartment contains polyphosphate and metals and is a specialized vacuolar structure based on proteomic analysis of *Cyanidioschyzon merolae* acidocalcisomes that identified V-ATPase subunits (Yagisawa et al., 2009). In addition, at least two candidate metal transporters, including a protein related to *S. cerevisiae* Ccc1 and a cation diffusion facilitator family member (putative Zn transporter), were described.

Cre02.g107550 encodes a protein related to *S. cerevisiae* Ccc1p and *Arabidopsis* VIT1. Yeast Ccc1p and plant VIT1 are vacuolar membrane proteins involved in transport of iron from the cytosol into the vacuoles (Li et al., 2001; Kim et al., 2006). Although the upregulation of *C. reinhardtii* CCC1-like seems counterintuitive, it is possible that it functions under iron deficiency to only transiently store the potentially toxic iron released from degraded or damaged iron-sulfur proteins into the vacuoles prior to its redistribution to intracellular compartments. A similar pattern of expression and function have been documented for a vacuolar zinc transporter in *S. cerevisiae* (ZRC1) (MacDiarmid et al., 2003). The pattern of expression of *C. reinhardtii CCC1* is consistent with the similar counterintuitive upregulation of chloroplast ferritin in iron deficiency, which has been demonstrated to function as a chloroplast iron buffer during remodeling of the photosynthetic apparatus in iron-starved cells (Busch et al., 2008; Long et al., 2008).

Cre16.g687000 encodes a ferroportin-like protein (FPN1). Similar expression profiles have been observed for plant ferroportin IREG2/FPN2 and IREG3/MAR1 (Table 4) (Colangelo and Guerinot, 2004; Buckhout et al., 2009; Zheng et al., 2009; Long et al., 2010; Yang et al., 2010). *Arabidopsis* FPN2 is localized to vacuolar membranes and MAR1 to the plastid envelope membranes. The proteins can apparently transport divalent cations like Co^{2+} and Ni^{2+}, besides Fe^{2+} (Schaaf et al., 2006; Conte et al., 2009; Morrissey et al., 2009). Among the likely functions are provision of iron to the plastid or

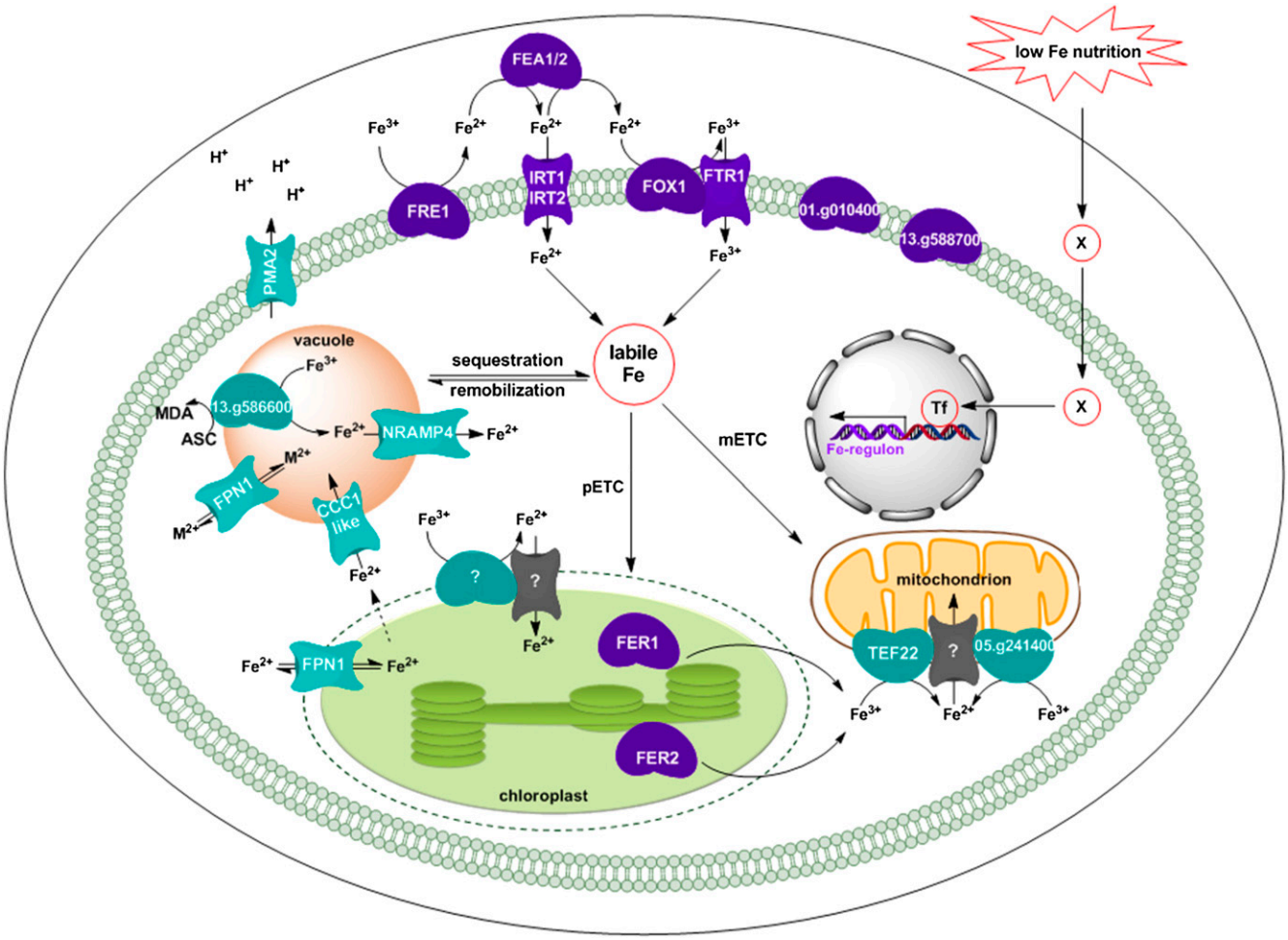

Figure 9. A Model for Signaling and Response to Poor Iron Nutrition in *C. reinhardtii*.

The signal, shown as x, is unknown, as is/are the transcription factor(s) (Tf). The vacuole may be identical to the previously described acidocalcisome (see text). Iron homeostasis components whose function is consistent with experimental documentation (localization and expression) are shown in purple, while those whose functions are more hypothetical (and identified in this study) are shown in turquoise. The identity of the labile iron (Fe) pool is not known. Transporters involved in Fe^{2+} import into chloroplast and mitochondria are not known (gray). mETC, mitochondrial electron transfer chain; pETC, photosynthetic electron transfer chain.

sequestration of other divalent cations to the vacuole. The latter function is necessary in iron-deficient cells because members of the ZIP family (like IRT1/2, which are induced) are not as selective for iron as is the FTR1/FOX1 pathway and may bring in unwanted, potentially toxic, ions. For instance, plant IRT proteins are known to transport Cd^{2+} (Connolly et al., 2002). In this context, it is worth noting the upregulation of glutathione and phytochelatin synthesis (Table 1), which detoxify cadmium by sequestration of Cd-PC complexes (Howe and Merchant, 1992; Clemens, 2006). Interestingly, a gene encoding a ferric-reductase–like protein (Cre05.g241400) is also upregulated. This could function to reduce intracellular ferric to ferrous prior to transport into the vacuole or the chloroplast, by analogy to Fre6p in yeast or FRO7 in *Arabidopsis* (Singh et al., 2007; Jeong et al., 2008).

There are three genes encoding cytochrome b_{561} family proteins (*TEF22*, *Cre14.g609900*, and *Cre13.g586600*). TEF22 and Cre14.g609900 have a DOMON domain fused to a cytochrome b_{561} ferric-reductase domain and are more related to mammalian FRRS-like ferric-reductases than they are to plant homologs (see Supplemental Figure 5 online). Mouse, rat, human, and *Drosophila melanogaster* SDR2 (FRRS1) are indeed functional ferric reductases, and mouse SDR2 is also regulated by iron (Vargas et al., 2003). Expression of mammalian duodenal cytochrome *b* (Dcyt*b*), which generates the Fe^{2+} used by DCT1/DMT1, is likewise regulated by iron nutrition (McKie et al., 2001; McKie, 2008), and two other mammalian cytochrome b_{561} homologs from chromaffin granules and lysosomes function as ascorbate-dependent ferric-reductases (Njus et al., 1987; Fleming and Kent, 1991; Fleming et al., 1997; Su and Asard, 2006; Zhang et al., 2006). These cytochrome b_{561} ferric-reductases each possess four conserved His residues involved in coordination of two heme molecules and conserved sites for ascorbate and

monodehydroascorbate binding (Trost et al., 2000; Takeuchi et al., 2004; Su and Asard, 2006). The *C. reinhardtii* proteins retain the conserved residues, making them likely to be true ferrir-eductases (see Supplemental Figures 4 and 5 online).

Proteomic studies indicated that TEF22 is in the mitochondrion (Allmer et al., 2006; Atteia et al., 2009), whereas localization prediction programs (WolfPsort) place Cre14.g609900 and Cre13.g586600 at the plasma membrane. Cre13.g586600 does not contain a DOMON domain and is homologous to ascorbate-dependent cytochrome b_{561} ferric-reductases. Thus, we propose that TEF22 is a ferric-reductase involved in supplying ferrous iron for mitochondrial respiratory complexes, whereas Cre14.g609900 may work with FRE1 at the plasma membrane. Note that TEF22 is always more highly expressed in acetate- versus CO_2-grown cells, consistent with the proposed function. In the case of Cre13.g586600, whose monodehydroascorbate and ascorbate binding sites are well conserved, it is possible that it could function in ascorbate regeneration from monodehydroascorbate at the plasma membrane or vacuolar membrane.

Regulation of Iron Homeostasis

In higher plants, a number of transcription factors have been identified as components of the iron signaling response, including FIT1/FER, PYE, bHLH115, and ILR3 (Ling et al., 2002; Colangelo and Guerinot, 2004; Brumbarova and Bauer, 2005; Bauer et al., 2007; Dinneny et al., 2008; Jeong and Guerinot, 2009; Long et al., 2010). In addition, there is a posttranslational component involving an E3 ubiquitin ligase BTS (Long et al., 2010). The conservation of BTS in *C. reinhardtii* (Cre05.g248550) and the identification of a bHLH transcription factor (Cre24g.7700450) whose expression is induced in iron-deficient *C. reinhardtii*, suggests that the signaling pathway is conserved despite the years of evolutionary distance (Tables 1 and 4). This is analogous to the situation for both Cu and P signaling where the *C. reinhardtii* proteins have orthologs with similar function in *Arabidopsis* (Wykoff et al., 1999; Rubio et al., 2001; Kropat et al., 2005; Yamasaki et al., 2009; Bernal et al., 2012). CDJ3/5 (which are unique to chloroplast-containing organisms), may also serve a posttranslational role, for instance in the regulated assembly of chloroplast iron-containing proteins (Dorn et al., 2010). The Fe/S site in these J-domain proteins may be iron-sensors. Unlike copper signaling in *C. reinhardtii*, where there is a single master regulator, iron signaling appears to be more complex. There are multiple types of FeREs and genes that respond with different kinetics or sensitivity to iron, indicating a complex network of iron sensing and signaling.

METHODS

Strains and Culture Conditions

Chlamydomonas reinhardtii strain 2137 (wild type, *mt*$^-$) was a gift from Laurens Mets (Spreitzer and Mets, 1981) and has been deposited at the Chlamydomonas Culture collection under accession CC-4532. The strain was grown in Tris-acetate-phosphate (TAP) or minimal medium (TP) with Hutner's trace elements (Harris, 2009; Terauchi et al., 2010) at 24°C and 50 to 100 μmol m^{-2} s^{-1} photon flux density. Iron nutritional stages were achieved by maintaining the strain in standard TAP medium (20 μM iron) and then transferred to iron-free TAP (or TP) supplemented with Fe-EDTA at the indicated concentrations as described (Moseley et al., 2002). The minimal medium (i.e., CO_2-grown) cultures were bubbled constantly with air. The metadata associated with the RNA-Seq experiments is available at http://genomes.mcdb.ucla.edu/CreIron/.

Plant Material and Growth Conditions

Arabidopsis thaliana ecotype Col-4 was used as the wild type. A mutant with a T-DNA insert in the *CGLD27* gene (At5g67370) was obtained from the Salk T-DNA collection (SALK_023292). Plants were grown (50 µmol m^{-2} s^{-1}, 12-h-light/12-h-dark cycle) at 23°C on 0.8% agar-solidified Murashige and Skoog medium including 1% Suc (Fisher Scientific) with various concentrations of $FeCl_3$ as indicated.

Nucleic Acid Analysis

Total RNA was extracted from exponentially grown *C. reinhardtii* cells as described previously (Quinn and Merchant, 1998). RNA quality was assessed on an Agilent 2100 bioanalyzer and by RNA hybridization as described (Allen et al., 2007a). The probe used for detection of *CBLP* was a 915-bp *Eco*RI fragment from the cDNA insert in plasmid pcf8-13 (Schloss, 1990). cDNA synthesis and quantitative real-time PCR was performed on technical triplicates as described (Allen et al., 2007a) using gene-specific primers listed in Supplemental Table 1 online. The data are presented as the fold change in mRNA abundance, normalized to an endogenous reference gene (*CBLP* or *UBQ2*), relative to the sample grown in iron-replete (20 µM) TAP medium. The abundance of two reference genes, *CBLP* and *UBQ2*, did not change under the conditions tested. For RNA-Seq, total RNA preparations were sequenced at Illumina as pair-end 35-mers for photoheterotrophically grown samples and as single-end 100-mers for photoautotrophically grown cells. Raw and processed sequence files are available at the National Center for Biotechnology Information (NCBI) Gene Expression Omnibus (accession number GSE35305). Mapping the reads to the *C. reinhardtii* genome (version FM4 assembly, Augustus 10.2 annotation) and calculation of transcript abundances in RPKM were performed as described previously (Urzica et al., 2012). Fold changes were computed from the average expression levels of biological replicates after regularization (imputation) of missing values. Differential expression analysis was performed using the DESeq package (Anders and Huber, 2010). P values obtained from DESeq were adjusted for multiple testing using Benjamini-Hochberg correction (Benjamini and Hochberg, 1995) to control FDRs. Expression patterns of differentially expressed genes were clustered with the R package MBCluster.Seq (Y. Si, P. Liu, P. Li, and T.P. Brutnell, unpublished data), which implements a model-based clustering model based on a negative binomial distribution. The coverage graphs can be visualized at http://genomes.mcdb.ucla.edu/CreIron/.

Phylogenetic Analysis

Phylogenetic relationships were inferred using the Maximum Likelihood method based on the Whelan and Goldman model (Whelan and Goldman, 2001). The bootstrap consensus tree inferred from 1000 replicates (Felsenstein, 1985) is taken to represent the evolutionary history of the taxa analyzed. Branches corresponding to partitions reproduced in <50% bootstrap replicates are collapsed. The percentage (>75%) of replicate trees in which the associated taxa clustered together in the bootstrap test (1000 replicates) are shown next to the branches (Felsenstein, 1985). Initial trees for the heuristic search were obtained automatically as follows. When the number of common sites was <100 or less than one-fourth of the total number of sites, the maximum parsimony method was used; otherwise, BIONJ method with MCL distance matrix was used. The tree is drawn to scale, with branch lengths measured in the number of substitutions per site. All positions containing gaps and missing data were

eliminated. Evolutionary analyses were conducted in MEGA5 (Tamura et al., 2011). Sequence alignments are presented in Supplemental Data Sets 10 to 16 online.

Sequence Analysis

Alignments of protein homologs/orthologs were performed using MUSCLE (http://www.ebi.ac.uk/Tools/msa/muscle). Protein similarity networks were generated from an all-versus-all BLAST analysis (pairwise alignment between all pairs of proteins) as described (Blaby-Haas and Merchant, 2012).

Quantitative Proteome Analysis

C. reinhardtii strain 2137 (CC-4532) was grown photoheterotrophically (TAP) in the presence of 20 μM iron (replete), 1 μM iron (deficient), and 0.25 μM iron (limited) in triplicate cultures inoculated separately from three independent starter cultures. *C. reinhardtii* cells were collected at a density of $\sim 5 \times 10^6$ cells mL^{-1} by centrifugation at 3440*g* for 5 min at 4°C (JA-20 rotor; Beckman), washed with 10 mM sodium-phosphate, pH 7.0, collected by centrifugation, and resuspended in the same solution containing 1 mM PMSF and 5 mM EDTA to a final density of 4×10^8 cells mL^{-1}. Cells were broken by two slow freeze-thaw cycles from –80 to 4°C, and insoluble material was removed by centrifugation at 4°C (16,000*g* for 10 min [F-45-24-11 rotor, Eppendorf 5415R centrifuge] followed by 253,000*g* for 20 min [TLA-110 rotor; Beckman]). Approximately 30 μg of protein from each sample was separated by SDS-PAGE (4 to 12% NuPage Bis-Tris gels; Invitrogen). Each gel lane was sliced into ~3-mm bands and treated with trypsin (sequencing grade modified trypsin; Promega). The resulting tryptic peptides were extracted into a 50/50 water/acetonitrile solution containing 2.5% (v/v) formic acid and lyophilized. Peptides were resuspended in 1% formic acid containing 25 fmol/μL BSA trypsin digestion standard (MassPREP BSA Digestion Standard; Waters) and analyzed as previously described (Castruita et al., 2011). Peptides were analyzed using a Waters nanoAcquity ultraperformance liquid chromatograph coupled to a Waters Xevo quadrupole time-of-flight mass spectrometer. Peptides were separated on a 5-μm Symmetry C_{18} 180 μm × 20-mm reversed-phase trap column in line with a 1.7-μm BEH130, 75 μm × 100-mm reversed-phase C_{18} analytical column and eluted on a 60 min 3% acetonitrile/0.1% formic acid to 40% acetonitrile/0.1% formic acid gradient at a flow rate of 0.3 μL/min to the electrospray ionization mass spectrometer. The liquid chromatography mass spectrometer was operated in the mass spectrometry (Elevated Energy) (MS^E) data independent acquisition mode (Silva et al., 2006a, 2006b; Geromanos et al., 2009), a method that collects product and precursor data in parallel by continually switching the collision energy between low (6 eV) and elevated energy (ramped from 15 to 40 eV) during alternating scans (mass-to-charge ratio 50 to 2000). Product ions are correlated to precursor ions using reconstructed retention times (i.e., alignment of liquid chromatography retention times of the precursors and products) and chromatographic peak shapes. At least two 1-μL replicate injections from each gel band were analyzed by liquid chromatography–mass spectrometry.

Liquid chromatography–mass spectrometry raw data were processed, and peptides/proteins were identified and quantified using Protein Lynx Global Server (PLGS version 2.4; Waters) described by Li et al. (2009). Peptides were searched against the Augustus 10.2 protein database modified by replacement of some catalog models with individual user-curated models and supplemented with sequences for keratin, trypsin, BSA, and chloroplast and mitochondrial proteins from NCBI. Searches were limited to trypsin proteolysis fragments, and peptide precursor and product ion mass tolerances were set to 20 and 40 ppm, respectively. Other search parameters include minimum number of peptide matches (Castruita et al., 2011), minimum number of product ions per peptide (Geromanos et al., 2009), minimum number of product ions per protein (Geromanos et al., 2009), maximum number of missed tryptic cleavage sites (Geromanos et al., 2009), and maximum false positive rate (4%) (Li et al., 2009). Carbamidomethylation of Cys residues was set as a fixed modification, and Met oxidation, Asn and Gln deamidation, and N-terminal acetylation were set as variable modifications. For additional stringency, we required that a protein be detected in at least two different conditions to be considered identified and required that a protein be observed in two of three biological replicates in each condition to be considered quantifiable. The quality of replicates can be evaluated in Supplemental Data Set 7 online, sheet labeled "experimental replicates."

Quantification of protein levels was achieved by the addition of an internal protein standard (BSA trypsin digest standard) to which the data set is normalized and uses up to the three most abundant shared peptides as described (Silva et al., 2005, 2006a, 2006b) to determine protein abundance. Changes in protein abundance were then determined based on whether they showed a statistically significant ($P < 0.05$ by student's *t* test) increase or decrease in abundance of at least 2-fold in magnitude between the iron-replete and iron-limited conditions. Proteins that were detected in only one of the conditions were included in the analysis only if their abundances were over 20 μmol/cell. Therefore, 992 proteins were identified in this analysis, of which ~524 could be quantified reliably.

Monodehydroascorbate Reductase Activity

A total of 2×10^8 cells were collected by centrifugation at 2500*g* for 3 min and washed in 10 mM sodium phosphate, pH 7.0. For monodehydroascorbate reductase activity measurements, cells were washed in 50 mM Tris-Cl, pH 7.0, and resuspended in 100 μL extraction buffer containing 50 mM K-PO_4, pH 7.5, 1 mM DTT, and 10% glycerol. The cells were broken by three freeze/thaw cycles and the soluble extracts separated by centrifugation at 16,100*g* for 10 min at 4°C. Protein concentration was determined by the Lowry method against a bovine BSA standard. Monodehydroascorbate reductase (MDAR1) activity was determined as described previously (Miyake and Asada, 1992). The decrease in absorbance at 340 nm due to oxidation of NADH was monitored in a 1-mL reaction mixture containing 50 mM K-PO_4 buffer, pH 7.5, 0.25 mM NADH, 2.5 mM ascorbate, 10 μL *C. reinhardtii* cell extract containing ~35 to 50 μg of protein, and 0.5 units of ascorbate oxidase (from *Cucurbita* sp, EC 1.10.3.3, Sigma-Aldrich product A0157). The reaction was initiated by addition of ascorbate oxidase. The specific activity was calculated using the 6.22 mM^{-1} cm^{-1} extinction coefficient after the rate of nonspecific NADH oxidase was subtracted.

Ascorbate Measurement

Vitamin C content was measured as described previously (Urzica et al., 2012).

Immunoblot Analysis

Proteins were separated by denaturing PAGE (10 to 15% monomer), transferred to polyvinylidene fluoride, and detected as described (Chen et al., 2008). Primary antibody dilutions were ferroxidase (1:300) and CF_1, (1:10,000). The primary antibody was diluted in blocking buffer and incubated at room temperature for 90 min. A 1:3000 dilution of goat anti-rabbit alkaline phosphatase (Southern Biotech) in blocking buffer was used as the secondary antibody for colorimetric detection with nitroblue tetrazolium and 5-bromo-4-chloro-3-indolylphosphate.

Chlorophyll Content Determination and Fluorescence Emission Analysis

Chlorophyll was extracted, and its concentration was estimated as described (Moseley et al., 2002). Room temperature fluorescence

parameters were measured using an open FluorCam detector (Photon Systems Instruments). Fluorescence emissions were recorded from liquid cultures of cells after dark adaptation periods of at least 5 min. After measuring of the dark-adapted fluorescence level, F_0, to measure the maximum fluorescence level, F_m, an 800-ms duration pulse of saturating light radiation (>1800 μmol photon m^{-2} s^{-1}) was applied followed by a 40-ms delay in darkness and subsequently 10 ms of actinic illumination with saturating flashes at 20-ms intervals. The maximal photochemical efficiency of photosystem II (F_v/F_m) was calculated as $(F_m - F_0)/F_m$.

Gene Model Correction and Functional Annotation

To manually correct gene models, the JGI browser for the *C. reinhardtii* v4 draft genome assembly (http://genome.jgi-psf.org/Chlre4/) was accessed. RNA-Seq data and ESTs mapped against the *C. reinhardtii* v4 draft genome assembly (http://genomes.mcdb.ucla.edu/Cre454/) available on the University of California, Santa Cruz genome browser were accessed to compare gene models against transcriptome data. Gene models were corrected using predicted models, RNA-Seq data, ESTs, and protein homology as guides. Hypothetical proteins with poor coverage were ignored for the manual curation.

The protein sequences of all differentially expressed transcripts from Supplemental Data Set 2 online (acetate and photoheterotrophic) and Supplemental Data Set 3 online (CO_2 and photoautotrophic), respectively, were analyzed at the Pfam site (E-value 1×10^{-4}) and by individual BLASTp analysis at NCBI or Phytozome. The protein domains were grouped according to their function in 14 categories: unknown, other, nucleic acid metabolism, signaling, redox and stress response, transporters, kinases and phosphatases, cell structure and function, proteases, carbon metabolism, photosynthesis, lipid metabolism, respiration, and amino acid metabolism. Unknowns refer to protein sequences for which a domain could not be identified or if the domain was identified as having an unknown function. Domains that could not be classified in any specific category were grouped into the "others" category.

Accession Numbers

C. reinhardtii strain 2137 (wild type, *mt*$^-$) has been deposited at the Chlamydomonas Culture collection under accession number CC-4532. RNA-Seq data are available at the NCBI Gene Expression Omnibus under accession number GSE35305. Supplemental Data Sets 1 to 16 are available at datadryad.org under accession number doi:10.5061/dryad.7sq5c.

Supplemental Data

The following materials are available in the online version of this article.

Supplemental Figure 1. Common and Distinct Genes Targeted in Photoautotrophically versus Photoheterotrophically Grown *C. reinhardtii* Cells.

Supplemental Figure 2. Fold Changes Estimated from RNA-Seq versus Real-Time PCR Experiments Are Well Correlated.

Supplemental Figure 3. NRAMP4 Homologous Sequences Are Highly Conserved in Algae, Plants, and Animal Species.

Supplemental Figure 4. *C. reinhardtii* TEF22 Is Similar to Animal Ferric-Reductases.

Supplemental Figure 5. Sequence Analysis of Cyt b_{561} Domain-Containing Proteins.

Supplemental Figure 6. *C. reinhardtii* Genome Encodes Two VIT1-Like Proteins.

Supplemental Figure 7. *C. reinhardtii* Ferric Reductase-Like Protein (Cre05.g241400) Is Closely Related to Plant Ferric Reductases.

Supplemental Figure 8. *C. reinhardtii* Ferroportin Shows High Sequence Similarity to Algal, Plant, and Animal Ferroportins.

Supplemental Figure 9. Iron Limitation Induces Changes in Abundances of Transcripts Encoding Enzymes Required for Carotenoid Biosynthesis.

Supplemental Figure 10. Plant and Algal Hemerythrin-E3 Ligase-Like Proteins Are Highly Conserved.

Supplemental Figure 11. *C. reinhardtii* CGLD27 (Cre05.g237050) Shows High Sequence Similarity to Algal, Plant, and Cyanobacterial ycf36 Proteins.

Supplemental Figure 12. Promoter Analysis of Genes Differentially Expressed under Iron Deficiency.

Supplemental Figure 13. *C. reinhardtii* Basic Helix-Loop-Helix Transcription Factor (Cre24.g770450) Is Related to Subgroup IV of Plant bHLH Transcription Factors.

Supplemental Figure 14. Changes in mRNA Abundances of Genes Encoding the Enzymes of Tetrapyrrole Metabolism in *C. reinhardtii*.

Supplemental Table 1. Primer Sequences Used for Real-Time PCR.

Supplemental Data Set 1. Summary of RNA-Seq Statistics (Sheet1) and Transcript Abundance for All Augustus 10.2 *C. reinhardtii* Genes (Sheet 2).

Supplemental Data Set 2. Differentially Accumulating RNAs in Photoheterotrophic Conditions (Three Sheets).

Supplemental Data Set 3. Differentially Accumulating RNAs in Photoheterotrophic Conditions (Three Sheets).

Supplemental Data Set 4. Differentially Accumulating RNAs in Photoautotrophic versus Photoheterotrophic Conditions (10 Sheets).

Supplemental Data Set 5. Comparison of mRNA Abundances for Genes Encoding Metal Transporters.

Supplemental Data Set 6. Comparison of mRNA Abundances for Genes Encoding Enzymes of the Isoprenoid and Carotenoids Biosynthesis/Degradation Pathways.

Supplemental Data Set 7. Summary of Protein Abundances from MS^E Analysis (Two Sheets).

Supplemental Data Set 8. Comparison of mRNA Abundances for Genes Encoding Carbon Metabolism Proteins.

Supplemental Data Set 9. Comparison of mRNA Abundances for Genes Encoding Subunits of the Tetrapyrrole Biosynthesis and Degradation Pathways.

Supplemental Data Set 10. Amino Acid Sequence Alignment Used to Produce Figure 5B.

Supplemental Data Set 11. Amino Acid Sequence Alignment Used to Produce Supplemental Figure 5B.

Supplemental Data Set 12. Amino Acid Sequence Alignment Used to Produce Supplemental Figure 6B.

Supplemental Data Set 13. Amino Acid Sequence Alignment Used to Produce Supplemental Figure 7B.

Supplemental Data Set 14. Amino Acid Sequence Alignment Used to Produce Supplemental Figure 8B.

Supplemental Data Set 15. Amino Acid Sequence Alignment Used to Produce Supplemental Figure 10B.

Supplemental Data Set 16. Amino Acid Sequence Alignment Used to Produce Supplemental Figure 13B.

ACKNOWLEDGMENTS

This work was supported by the Division of Chemical Sciences, Geosciences, and Biosciences, Office of Basic Energy Sciences of the U.S.

Department of Energy (DE-FD02-04ER15529).The mass spectrometry and bioinformatic analyses of Illumina sequencing data were supported by the University of California–Los Angeles Department of Energy Institute of Genomics and Proteomics (DE-FC03-02ER63421 to J.A.L., S.S.M., and M.P.) and the analysis of ascorbate metabolism by the National Institutes of Health (GM026020 to S.G.C.). S.I.H. and S.J.K. acknowledge support from an Institutional Ruth L. Kirschstein National Research Service Award (GM07185), C.E.B.-H. from an Individual Kirschstein National Research Service Award (GM100753), L.N.A. from University of California–Los Angeles Graduate Division, and H.Y. from the Toyobo Foundation. We thank Janette Kropat and Martin Lohr for help with the figures on the chlorophyll and carotenoids metabolism pathways.

AUTHOR CONTRIBUTIONS

S.S.M. conceived the project. S.S.M., E.I.U, H.Y., and S.I.H. designed the experiments. E.I.U., H.Y., L.N.A., and S.I.H. performed the experiments. D.C. performed the bioinformatic analysis of RNA-Seq data and generated Figure 3B, Supplemental Figure 1D online, and Supplemental Figure 12 online. M.P supervised all bioinformatic analysis. S.J.K. and C.E.B.H. corrected gene models and generated Figure 8A and Figure 5, respectively. J.A.L. and S.G.C. contributed new analytical tools and designed experiments. S.S.M., E.I.U., L.N.A., and S.I.H. analyzed the data. S.S.M., and E.I.U. prepared the article. All authors commented on the article.

Received July 10, 2012; revised August 31, 2012; accepted September 12, 2012; published October 5, 2012.

REFERENCES

Allen, A.E., Laroche, J., Maheswari, U., Lommer, M., Schauer, N., Lopez, P.J., Finazzi, G., Fernie, A.R., and Bowler, C. (2008). Whole-cell response of the pennate diatom *Phaeodactylum tricornutum* to iron starvation. Proc. Natl. Acad. Sci. USA **105:** 10438–10443.

Allen, M.D., del Campo, J.A., Kropat, J., and Merchant, S.S. (2007a). *FEA1*, *FEA2*, and *FRE1*, encoding two homologous secreted proteins and a candidate ferrireductase, are expressed coordinately with *FOX1* and *FTR1* in iron-deficient *Chlamydomonas reinhardtii*. Eukaryot. Cell **6:** 1841–1852.

Allen, M.D., Kropat, J., Tottey, S., Del Campo, J.A., and Merchant, S.S. (2007b). Manganese deficiency in Chlamydomonas results in loss of photosystem II and MnSOD function, sensitivity to peroxides, and secondary phosphorus and iron deficiency. Plant Physiol. **143:** 263–277.

Allmer, J., Naumann, B., Markert, C., Zhang, M., and Hippler, M. (2006). Mass spectrometric genomic data mining: Novel insights into bioenergetic pathways in *Chlamydomonas reinhardtii*. Proteomics **6:** 6207–6220.

Anders, S., and Huber, W. (2010). Differential expression analysis for sequence count data. Genome Biol. **11:** R106.

Andrews, N.C. (2000). Iron homeostasis: Insights from genetics and animal models. Nat. Rev. Genet. **1:** 208–217.

Atteia, A., et al. (2009). A proteomic survey of *Chlamydomonas reinhardtii* mitochondria sheds new light on the metabolic plasticity of the organelle and on the nature of the alpha-proteobacterial mitochondrial ancestor. Mol. Biol. Evol. **26:** 1533–1548.

Bauer, P., Ling, H.Q., and Guerinot, M.L. (2007). FIT, the FER-LIKE IRON DEFICIENCY INDUCED TRANSCRIPTION FACTOR in Arabidopsis. Plant Physiol. Biochem. **45:** 260–261.

Behrenfeld, M.J., et al. (2009). Satellite-detected fluorescence reveals global physiology of ocean phytoplankton. Biogeosciences **6:** 779.

Benjamini, Y., and Hochberg, Y. (1995). Controlling the false discovery rate: A practical and powerful approach to multiple testing. J. R. Stat. Soc. Series B. Methodol. **57:** 289–300.

Bernal, M., Casero, D., Singh, V., Wilson, G.T., Grande, A., Yang, H., Dodani, S.C., Pellegrini, M., Huijser, P., Connolly, E.L., Merchant, S.S., and Krämer, U. (2012). Transcriptome sequencing identifies *SPL7*-regulated copper acquisition genes *FRO4*/*FRO5* and the copper dependence of iron homeostasis in *Arabidopsis*. Plant Cell **24:** 738–761.

Blaby-Haas, C.E., and Merchant, S.S. (2012). The ins and outs of algal metal transport. Biochim. Biophys. Acta **1823:** 1531–1552.

Briat, J.-F., and Lobréaux, S. (1997). Iron transport and storage in plants. Trends Plant Sci. **2:** 187–193.

Briat, J.F., Lobréaux, S., Grignon, N., and Vansuyt, G. (1999). Regulation of plant ferritin synthesis: How and why. Cell. Mol. Life Sci. **56:** 155–166.

Brumbarova, T., and Bauer, P. (2005). Iron-mediated control of the basic helix-loop-helix protein FER, a regulator of iron uptake in tomato. Plant Physiol. **137:** 1018–1026.

Buckhout, T.J., Yang, T.J., and Schmidt, W. (2009). Early iron-deficiency-induced transcriptional changes in Arabidopsis roots as revealed by microarray analyses. BMC Genomics **10:** 147.

Busch, A., Rimbauld, B., Naumann, B., Rensch, S., and Hippler, M. (2008). Ferritin is required for rapid remodeling of the photosynthetic apparatus and minimizes photo-oxidative stress in response to iron availability in *Chlamydomonas reinhardtii*. Plant J. **55:** 201–211.

de Benoist, B., McLean, E., Egli, I., and Cogswell, M., eds. (2008). Worldwide Prevalence of Anaemia 1993–2005: WHO Global Database on Anaemia. (WHO Press: Geneva, Switzerland).

Cardol, P., González-Halphen, D., Reyes-Prieto, A., Baurain, D., Matagne, R.F., and Remacle, C. (2005). The mitochondrial oxidative phosphorylation proteome of *Chlamydomonas reinhardtii* deduced from the Genome Sequencing Project. Plant Physiol. **137:** 447–459.

Cardol, P., Vanrobaeys, F., Devreese, B., Van Beeumen, J., Matagne, R.F., and Remacle, C. (2004). Higher plant-like subunit composition of mitochondrial complex I from *Chlamydomonas reinhardtii*: 31 conserved components among eukaryotes. Biochim. Biophys. Acta **1658:** 212–224.

Castruita, M., Casero, D., Karpowicz, S.J., Kropat, J., Vieler, A., Hsieh, S.I., Yan, W., Cokus, S., Loo, J.A., Benning, C., Pellegrini, M., and Merchant, S.S. (2011). Systems biology approach in *Chlamydomonas* reveals connections between copper nutrition and multiple metabolic steps. Plant Cell **23:** 1273–1292.

Chen, J.C., Hsieh, S.I., Kropat, J., and Merchant, S.S. (2008). A ferroxidase encoded by *FOX1* contributes to iron assimilation under conditions of poor iron nutrition in Chlamydomonas. Eukaryot. Cell **7:** 541–545.

Chen, Y.H., Wu, X.M., Ling, H.Q., and Yang, W.C. (2006). Transgenic expression of DwMYB2 impairs iron transport from root to shoot in *Arabidopsis thaliana*. Cell Res. **16:** 830–840.

Clemens, S. (2006). Toxic metal accumulation, responses to exposure and mechanisms of tolerance in plants. Biochimie **88:** 1707–1719.

Clemens, S., Naumann, B., and Hippler, M. (2009). Proteomics of metal mediated protein dynamics in plants - Iron and cadmium in the focus. Front. Biosci. **14:** 1955–1969.

Colangelo, E.P., and Guerinot, M.L. (2004). The essential basic helix-loop-helix protein FIT1 is required for the iron deficiency response. Plant Cell **16:** 3400–3412.

Connolly, E.L., Fett, J.P., and Guerinot, M.L. (2002). Expression of the IRT1 metal transporter is controlled by metals at the levels of transcript and protein accumulation. Plant Cell **14:** 1347–1357.

Conte, S., Stevenson, D., Furner, I., and Lloyd, A. (2009). Multiple antibiotic resistance in Arabidopsis is conferred by mutations in a chloroplast-localized transport protein. Plant Physiol. **151:** 559–573.

Courville, P., Chaloupka, R., and Cellier, M.F. (2006). Recent progress in structure-function analyses of Nramp proton-dependent metal-ion transporters. Biochem. Cell Biol. **84:** 960–978.

De Domenico, I., McVey Ward, D., and Kaplan, J. (2008). Regulation of iron acquisition and storage: Consequences for iron-linked disorders. Nat. Rev. Mol. Cell Biol. **9:** 72–81.

Deng, X., and Eriksson, M. (2007). Two iron-responsive promoter elements control expression of *FOX1* in *Chlamydomonas reinhardtii*. Eukaryot. Cell **6:** 2163–2167.

Dinneny, J.R., Long, T.A., Wang, J.Y., Jung, J.W., Mace, D., Pointer, S., Barron, C., Brady, S.M., Schiefelbein, J., and Benfey, P.N. (2008). Cell identity mediates the response of Arabidopsis roots to abiotic stress. Science **320:** 942–945.

Dorn, K.V., Willmund, F., Schwarz, C., Henselmann, C., Pohl, T., Hess, B., Veyel, D., Usadel, B., Friedrich, T., Nickelsen, J., and Schroda, M. (2010). Chloroplast DnaJ-like proteins 3 and 4 (CDJ3/4) from *Chlamydomonas reinhardtii* contain redox-active Fe-S clusters and interact with stromal HSP70B. Biochem. J. **427:** 205–215.

Douglas, S.E., and Penny, S.L. (1999). The plastid genome of the cryptophyte alga, *Guillardia theta*: Complete sequence and conserved synteny groups confirm its common ancestry with red algae. J. Mol. Evol. **48:** 236–244.

Fang, W., Si, Y., Douglass, S., Casero, D., Merchant, S.S., Pellegrini, M., Ladunga, I., Liu, P., and Spalding, M.H. (2012). Transcriptome-wide changes in *Chlamydomonas reinhardtii* gene expression regulated by carbon dioxide and the CO_2-concentrating mechanism regulator *CIA5/CCM1*. Plant Cell **24:** 1876–1893.

Fei, X., and Deng, X. (2007). A novel Fe deficiency-responsive element (FeRE) regulates the expression of *atx1* in *Chlamydomonas reinharditii*. Plant Cell Physiol. **48:** 1496–1503.

Fei, X., Eriksson, M., Li, Y., and Deng, X. (2010). A novel negative Fe-deficiency-responsive element and a TGGCA-type-like FeRE control the expression of *FTR1* in *Chlamydomonas reinhardtii*. J. Biomed. Biotechnol. **2010:** 790247.

Fei, X., Eriksson, M., Yang, J., and Deng, X. (2009). An Fe deficiency responsive element with a core sequence of TGGCA regulates the expression of *FEA1* in *Chlamydomonas reinharditii*. J. Biochem. **146:** 157–166.

Felsenstein, J. (1985). Confidence limits on phylogenies: An approach using the bootstrap. Evolution **39:** 783–791.

Fleming, M.D., Trenor, C.C., IIISu, M.A., Foernzler, D., Beier, D.R., Dietrich, W.F., and Andrews, N.C. (1997). Microcytic anaemia mice have a mutation in Nramp2, a candidate iron transporter gene. Nat. Genet. **16:** 383–386.

Fleming, P.J., and Kent, U.M. (1991). Cytochrome b_{561}, ascorbic acid, and transmembrane electron transfer. Am. J. Clin. Nutr. **54**(6, Suppl) 1173S–1178S.

Foyer, C.H., and Noctor, G. (2011). Ascorbate and glutathione: The heart of the redox hub. Plant Physiol. **155:** 2–18.

Geromanos, S.J., Vissers, J.P., Silva, J.C., Dorschel, C.A., Li, G.Z., Gorenstein, M.V., Bateman, R.H., and Langridge, J.I. (2009). The detection, correlation, and comparison of peptide precursor and product ions from data independent LC-MS with data dependant LC-MS/MS. Proteomics **9:** 1683–1695.

Gill, S.S., and Tuteja, N. (2010). Reactive oxygen species and antioxidant machinery in abiotic stress tolerance in crop plants. Plant Physiol. Biochem. **48:** 909–930.

Guerinot, M.L., and Yi, Y. (1994). Iron: Nutritious, noxious, and not readily available. Plant Physiol. **104:** 815–820.

Harris, E.H. (2009). The Chlamydomonas Sourcebook, 2nd ed. (San Diego, CA: Academic Press).

Hell, R., and Stephan, U.W. (2003). Iron uptake, trafficking and homeostasis in plants. Planta **216:** 541–551.

Hellman, N.E., and Gitlin, J.D. (2002). Ceruloplasmin metabolism and function. Annu. Rev. Nutr. **22:** 439–458.

Howe, G., and Merchant, S. (1992). Heavy metal-activated synthesis of peptides in *Chlamydomonas reinhardtii*. Plant Physiol. **98:** 127–136.

Jakoby, M., Wang, H.Y., Reidt, W., Weisshaar, B., and Bauer, P. (2004). *FRU* (*BHLH029*) is required for induction of iron mobilization genes in *Arabidopsis thaliana*. FEBS Lett. **577:** 528–534.

Jeong, J., Cohu, C., Kerkeb, L., Pilon, M., Connolly, E.L., and Guerinot, M.L. (2008). Chloroplast Fe(III) chelate reductase activity is essential for seedling viability under iron limiting conditions. Proc. Natl. Acad. Sci. USA **105:** 10619–10624.

Jeong, J., and Guerinot, M.L. (2009). Homing in on iron homeostasis in plants. Trends Plant Sci. **14:** 280–285.

Karpowicz, S.J., Prochnik, S.E., Grossman, A.R., and Merchant, S.S. (2011). The GreenCut2 resource, a phylogenomically derived inventory of proteins specific to the plant lineage. J. Biol. Chem. **286:** 21427–21439.

Kim, S.A., Punshon, T., Lanzirotti, A., Li, L., Alonso, J.M., Ecker, J.R., Kaplan, J., and Guerinot, M.L. (2006). Localization of iron in Arabidopsis seed requires the vacuolar membrane transporter VIT1. Science **314:** 1295–1298.

Kosman, D.J. (2010). Redox cycling in iron uptake, efflux, and trafficking. J. Biol. Chem. **285:** 26729–26735.

Kourmpetis, Y.A., van Dijk, A.D., Bink, M.C., van Ham, R.C., and ter Braak, C.J. (2010). Bayesian Markov Random Field analysis for protein function prediction based on network data. PLoS ONE **5:** e9293.

Kropat, J., Tottey, S., Birkenbihl, R.P., Depège, N., Huijser, P., and Merchant, S. (2005). A regulator of nutritional copper signaling in Chlamydomonas is an SBP domain protein that recognizes the GTAC core of copper response element. Proc. Natl. Acad. Sci. USA **102:** 18730–18735.

La Fontaine, S., Quinn, J.M., Nakamoto, S.S., Page, M.D., Göhre, V., Moseley, J.L., Kropat, J., and Merchant, S. (2002). Copper-dependent iron assimilation pathway in the model photosynthetic eukaryote *Chlamydomonas reinhardtii*. Eukaryot. Cell **1:** 736–757.

Lanquar, V., Lelièvre, F., Bolte, S., Hamès, C., Alcon, C., Neumann, D., Vansuyt, G., Curie, C., Schröder, A., Krämer, U., Barbier-Brygoo, H., and Thomine, S. (2005). Mobilization of vacuolar iron by AtNRAMP3 and AtNRAMP4 is essential for seed germination on low iron. EMBO J. **24:** 4041–4051.

Li, G.Z., Vissers, J.P., Silva, J.C., Golick, D., Gorenstein, M.V., and Geromanos, S.J. (2009). Database searching and accounting of multiplexed precursor and product ion spectra from the data independent analysis of simple and complex peptide mixtures. Proteomics **9:** 1696–1719.

Li, J., Wu, X.D., Hao, S.T., Wang, X.J., and Ling, H.Q. (2008). Proteomic response to iron deficiency in tomato root. Proteomics **8:** 2299–2311.

Li, L., Chen, O.S., McVey Ward, D., and Kaplan, J. (2001). CCC1 is a transporter that mediates vacuolar iron storage in yeast. J. Biol. Chem. **276:** 29515–29519.

Lill, R., and Mühlenhoff, U. (2008). Maturation of iron-sulfur proteins in eukaryotes: Mechanisms, connected processes, and diseases. Annu. Rev. Biochem. **77:** 669–700.

Ling, H.Q., Bauer, P., Bereczky, Z., Keller, B., and Ganal, M. (2002). The tomato *fer* gene encoding a bHLH protein controls iron-uptake responses in roots. Proc. Natl. Acad. Sci. USA **99:** 13938–13943.

Linster, C.L., Gomez, T.A., Christensen, K.C., Adler, L.N., Young, B.D., Brenner, C., and Clarke, S.G. (2007). Arabidopsis *VTC2* encodes a GDP-L-galactose phosphorylase, the last unknown enzyme

in the Smirnoff-Wheeler pathway to ascorbic acid in plants. J. Biol. Chem. **282:** 18879–18885.

Livak, K.J., and Schmittgen, T.D. (2001). Analysis of relative gene expression data using real-time quantitative PCR and the 2(-Delta Delta C(T)) method. Methods **25:** 402–408.

Lohr, M., Im, C.S., and Grossman, A.R. (2005). Genome-based examination of chlorophyll and carotenoid biosynthesis in *Chlamydomonas reinhardtii*. Plant Physiol. **138:** 490–515.

Lohr, M., Schwender, J., and Polle, J.E. (2012). Isoprenoid biosynthesis in eukaryotic phototrophs: A spotlight on algae. Plant Sci. **185-186:** 9–22.

Long, J.C., Sommer, F., Allen, M.D., Lu, S.F., and Merchant, S.S. (2008). *FER1* and *FER2* encoding two ferritin complexes in *Chlamydomonas reinhardtii* chloroplasts are regulated by iron. Genetics **179:** 137–147.

Long, T.A., Tsukagoshi, H., Busch, W., Lahner, B., Salt, D.E., and Benfey, P.N. (2010). The bHLH transcription factor POPEYE regulates response to iron deficiency in *Arabidopsis* roots. Plant Cell **22:** 2219–2236.

MacDiarmid, C.W., Milanick, M.A., and Eide, D.J. (2003). Induction of the ZRC1 metal tolerance gene in zinc-limited yeast confers resistance to zinc shock. J. Biol. Chem. **278:** 15065–15072.

McKie, A.T. (2008). The role of Dcytb in iron metabolism: An update. Biochem. Soc. Trans. **36:** 1239–1241.

McKie, A.T., et al. (2001). An iron-regulated ferric reductase associated with the absorption of dietary iron. Science **291:** 1755–1759.

Merchant, S.S., Allen, M.D., Kropat, J., Moseley, J.L., Long, J.C., Tottey, S., and Terauchi, A.M. (2006). Between a rock and a hard place: Trace element nutrition in Chlamydomonas. Biochim. Biophys. Acta **1763:** 578–594.

Merchant, S.S., and Helmann, J.D. (2012). Elemental economy: Microbial strategies for optimizing growth in the face of nutrient limitation. Adv. Microb. Physiol. **60:** 91–210.

Miyake, C., and Asada, K. (1992). Thylakoid-bound ascorbate peroxidase in spinach chloroplasts and photoreduction of its primary oxidation product monodehydroascorbate radicals in thylakoids. Plant Cell Physiol. **33:** 541–553.

Morel, F.M.M., Hudson, R.J.M., and Price, N.M. (1991). Limitation of productivity by trace metals in the sea. Limnol. Oceanogr. **36:** 1742.

Morrissey, J., Baxter, I.R., Lee, J., Li, L., Lahner, B., Grotz, N., Kaplan, J., Salt, D.E., and Guerinot, M.L. (2009). The ferroportin metal efflux proteins function in iron and cobalt homeostasis in *Arabidopsis*. Plant Cell **21:** 3326–3338.

Morrissey, J., and Guerinot, M.L. (2009). Iron uptake and transport in plants: The good, the bad, and the ionome. Chem. Rev. **109:** 4553–4567.

Mortazavi, A., Williams, B.A., McCue, K., Schaeffer, L., and Wold, B. (2008). Mapping and quantifying mammalian transcriptomes by RNA-Seq. Nat. Methods **5:** 621–628.

Moseley, J.L., Allinger, T., Herzog, S., Hoerth, P., Wehinger, E., Merchant, S., and Hippler, M. (2002). Adaptation to Fe-deficiency requires remodeling of the photosynthetic apparatus. EMBO J. **21:** 6709–6720.

Naumann, B., Busch, A., Allmer, J., Ostendorf, E., Zeller, M., Kirchhoff, H., and Hippler, M. (2007). Comparative quantitative proteomics to investigate the remodeling of bioenergetic pathways under iron deficiency in *Chlamydomonas reinhardtii*. Proteomics **7:** 3964–3979.

Naumann, B., Stauber, E.J., Busch, A., Sommer, F., and Hippler, M. (2005). N-terminal processing of Lhca3 Is a key step in remodeling of the photosystem I-light-harvesting complex under iron deficiency in *Chlamydomonas reinhardtii*. J. Biol. Chem. **280:** 20431–20441.

Nevo, Y., and Nelson, N. (2006). The NRAMP family of metal-ion transporters. Biochim. Biophys. Acta **1763:** 609–620.

Njus, D., Kelley, P.M., Harnadek, G.J., and Pacquing, Y.V. (1987). Mechanism of ascorbic acid regeneration mediated by cytochrome b_{561}. Ann. N. Y. Acad. Sci. **493:** 108–119.

Obayashi, T., Kinoshita, K., Nakai, K., Shibaoka, M., Hayashi, S., Saeki, M., Shibata, D., Saito, K., and Ohta, H. (2007). ATTED-II: A database of co-expressed genes and cis elements for identifying co-regulated gene groups in Arabidopsis. Nucleic Acids Res. **35** (Database issue)**:** D863–D869.

Obayashi, T., Nishida, K., Kasahara, K., and Kinoshita, K. (2011). ATTED-II updates: Condition-specific gene coexpression to extend coexpression analyses and applications to a broad range of flowering plants. Plant Cell Physiol. **52:** 213–219.

Ogo, Y., Itai, R.N., Nakanishi, H., Inoue, H., Kobayashi, T., Suzuki, M., Takahashi, M., Mori, S., and Nishizawa, N.K. (2006). Isolation and characterization of IRO2, a novel iron-regulated bHLH transcription factor in graminaceous plants. J. Exp. Bot. **57:** 2867–2878.

Page, M.D., Allen, M.D., Kropat, J., Urzica, E.I., Karpowicz, S.J., Hsieh, S.I., Loo, J.A., and Merchant, S.S. (2012). Fe sparing and Fe recycling contribute to increased superoxide dismutase capacity in iron-starved *Chlamydomonas reinhardtii*. Plant Cell **24:** 2649–2665.

Philpott, C.C. (2006). Iron uptake in fungi: A system for every source. Biochim. Biophys. Acta **1763:** 636–645.

Philpott, C.C., and Protchenko, O. (2008). Response to iron deprivation in *Saccharomyces cerevisiae*. Eukaryot. Cell **7:** 20–27.

Portnoy, M.E., Liu, X.F., and Culotta, V.C. (2000). *Saccharomyces cerevisiae* expresses three functionally distinct homologues of the nramp family of metal transporters. Mol. Cell. Biol. **20:** 7893–7902.

Quinn, J.M., and Merchant, S. (1998). Copper-responsive gene expression during adaptation to copper deficiency. Methods Enzymol. **297:** 263–279.

Rampey, R.A., Woodward, A.W., Hobbs, B.N., Tierney, M.P., Lahner, B., Salt, D.E., and Bartel, B. (2006). An Arabidopsis basic helix-loop-helix leucine zipper protein modulates metal homeostasis and auxin conjugate responsiveness. Genetics **174:** 1841–1857.

Reinhardt, I., Haebel, S., Herbik, A., and Buckhout, T.J. (2006). Proteomic studies under iron stress: Iron deficiency-induced regulation of protein synthesis in the green alga *Chlamydomonas reinhardtii*. In Iron Nutrition in Plants and Rhizospheric Microorganisms, L.L. Barton and J. Abadia, eds (Dordrecht, The Netherlands: Springer), pp. 371–393.

Riedel, H.D., Remus, A.J., Fitscher, B.A., and Stremmel, W. (1995). Characterization and partial purification of a ferrireductase from human duodenal microvillus membranes. Biochem. J. **309:** 745–748.

Rubio, V., Linhares, F., Solano, R., Martín, A.C., Iglesias, J., Leyva, A., and Paz-Ares, J. (2001). A conserved MYB transcription factor involved in phosphate starvation signaling both in vascular plants and in unicellular algae. Genes Dev. **15:** 2122–2133.

Ruiz, F.A., Marchesini, N., Seufferheld, M., Govindjee, Docampo, R. (2001). The polyphosphate bodies of *Chlamydomonas reinhardtii* possess a proton-pumping pyrophosphatase and are similar to acidocalcisomes. J. Biol. Chem. **276:** 46196–46203.

Salahudeen, A.A., Thompson, J.W., Ruiz, J.C., Ma, H.W., Kinch, L.N., Li, Q., Grishin, N.V., and Bruick, R.K. (2009). An E3 ligase possessing an iron-responsive hemerythrin domain is a regulator of iron homeostasis. Science **326:** 722–726.

Santi, S., and Schmidt, W. (2009). Dissecting iron deficiency-induced proton extrusion in Arabidopsis roots. New Phytol. **183:** 1072–1084.

Schaaf, G., Honsbein, A., Meda, A.R., Kirchner, S., Wipf, D., and von Wirén, N. (2006). *AtIREG2* encodes a tonoplast transport protein involved in iron-dependent nickel detoxification in *Arabidopsis thaliana* roots. J. Biol. Chem. **281:** 25532–25540.

Schloss, J.A. (1990). A Chlamydomonas gene encodes a G protein beta subunit-like polypeptide. Mol. Gen. Genet. **221:** 443–452.

Schmid, M., Davison, T.S., Henz, S.R., Pape, U.J., Demar, M., Vingron, M., Schölkopf, B., Weigel, D., and Lohmann, J.U. (2005). A gene expression map of *Arabidopsis thaliana* development. Nat. Genet. **37:** 501–506.

Schuler, M., Keller, A., Backes, C., Philippar, K., Lenhof, H.P., and Bauer, P. (2011). Transcriptome analysis by GeneTrail revealed regulation of functional categories in response to alterations of iron homeostasis in *Arabidopsis thaliana*. BMC Plant Biol. **11:** 87.

Schultz, I.J., Chen, C., Paw, B.H., and Hamza, I. (2010). Iron and porphyrin trafficking in heme biogenesis. J. Biol. Chem. **285:** 26753–26759.

Shen, J., Xu, X., Li, T., Cao, D., and Han, Z. (2008). An MYB transcription factor from *Malus xiaojinensis* has a potential role in iron nutrition. J. Integr. Plant Biol. **50:** 1300–1306.

Silva, J.C., Denny, R., Dorschel, C.A., Gorenstein, M., Kass, I.J., Li, G.Z., McKenna, T., Nold, M.J., Richardson, K., Young, P., and Geromanos, S. (2005). Quantitative proteomic analysis by accurate mass retention time pairs. Anal. Chem. **77:** 2187–2200.

Silva, J.C., Denny, R., Dorschel, C., Gorenstein, M.V., Li, G.Z., Richardson, K., Wall, D., and Geromanos, S.J. (2006a). Simultaneous qualitative and quantitative analysis of the *Escherichia coli* proteome: A sweet tale. Mol. Cell Proteomics **5:** 589–607.

Silva, J.C., Gorenstein, M.V., Li, G.Z., Vissers, J.P., and Geromanos, S.J. (2006b). Absolute quantification of proteins by LCMS^{E}: A virtue of parallel MS acquisition. Mol. Cell. Proteomics **5:** 144–156.

Singh, A., Kaur, N., and Kosman, D.J. (2007). The metalloreductase Fre6p in Fe-efflux from the yeast vacuole. J. Biol. Chem. **282:** 28619–28626.

Sonnhammer, E.L., von Heijne, G., and Krogh, A. (1998). A hidden Markov model for predicting transmembrane helices in protein sequences. Proc. Int. Conf. Intell. Syst. Mol. Biol. **6:** 175–182.

Sperotto, R.A., Boff, T., Duarte, G.L., and Fett, J.P. (2008). Increased senescence-associated gene expression and lipid peroxidation induced by iron deficiency in rice roots. Plant Cell Rep. **27:** 183–195.

Spiller, S.C., Castelfranco, A.M., and Castelfranco, P.A. (1982). Effects of iron and oxygen on chlorophyll biosynthesis: I. *In vivo* observations on iron and oxygen-deficient plants. Plant Physiol. **69:** 107–111.

Spreitzer, R.J., and Mets, L. (1981). Photosynthesis-deficient mutants of *Chlamydomonas reinhardtii* with associated light-sensitive phenotypes. Plant Physiol. **67:** 565–569.

Staiger, D. (2002). Chemical strategies for iron acquisition in plants. Angew. Chem. Int. Ed. Engl. **41:** 2259–2264.

Stanke, M., Diekhans, M., Baertsch, R., and Haussler, D. (2008). Using native and syntenically mapped cDNA alignments to improve *de novo* gene finding. Bioinformatics **24:** 637–644.

Stein, R.J., and Waters, B.M. (2012). Use of natural variation reveals core genes in the transcriptome of iron-deficient *Arabidopsis thaliana* roots. J. Exp. Bot. **63:** 1039–1055.

Su, D., and Asard, H. (2006). Three mammalian cytochromes b_{561} are ascorbate-dependent ferrireductases. FEBS J. **273:** 3722–3734.

Takeuchi, F., Hori, H., Obayashi, E., Shiro, Y., and Tsubaki, M. (2004). Properties of two distinct heme centers of cytochrome b_{561} from bovine chromaffin vesicles studied by EPR, resonance Raman, and ascorbate reduction assay. J. Biochem. **135:** 53–64.

Tamura, K., Peterson, D., Peterson, N., Stecher, G., Nei, M., and Kumar, S. (2011). MEGA5: Molecular evolutionary genetics analysis using maximum likelihood, evolutionary distance, and maximum parsimony methods. Mol. Biol. Evol. **28:** 2731–2739.

Terauchi, A.M., Lu, S.F., Zaffagnini, M., Tappa, S., Hirasawa, M., Tripathy, J.N., Knaff, D.B., Farmer, P.J., Lemaire, S.D., Hase, T., and Merchant, S.S. (2009). Pattern of expression and substrate specificity of chloroplast ferredoxins from *Chlamydomonas reinhardtii*. J. Biol. Chem. **284:** 25867–25878.

Terauchi, A.M., Peers, G., Kobayashi, M.C., Niyogi, K.K., and Merchant, S.S. (2010). Trophic status of *Chlamydomonas reinhardtii* influences the impact of iron deficiency on photosynthesis. Photosynth. Res. **105:** 39–49.

Thamatrakoln, K., Korenovska, O., Niheu, A.K., and Bidle, K.D. (2012). Whole-genome expression analysis reveals a role for death-related genes in stress acclimation of the diatom *Thalassiosira pseudonana*. Environ. Microbiol. **14:** 67–81.

Theil, E.C. (2004). Iron, ferritin, and nutrition. Annu. Rev. Nutr. **24:** 327–343.

Thomine, S., Lelièvre, F., Debarbieux, E., Schroeder, J.I., and Barbier-Brygoo, H. (2003). AtNRAMP3, a multispecific vacuolar metal transporter involved in plant responses to iron deficiency. Plant J. **34:** 685–695.

Thomine, S., Wang, R., Ward, J.M., Crawford, N.M., and Schroeder, J.I. (2000). Cadmium and iron transport by members of a plant metal transporter family in Arabidopsis with homology to Nramp genes. Proc. Natl. Acad. Sci. USA **97:** 4991–4996.

Trost, P., Bèrczi, A., Sparla, F., Sponza, G., Marzadori, B., Asard, H., and Pupillo, P. (2000). Purification of cytochrome b-$_{561}$ from bean hypocotyls plasma membrane. Evidence for the presence of two heme centers. Biochim. Biophys. Acta **1468:** 1–5.

Urzica, E.I., Adler, L.N., Page, M.D., Linster, C.L., Arbing, M.A., Casero, D., Pellegrini, M., Merchant, S.S., and Clarke, S.G. (2012). Impact of oxidative stress on ascorbate biosynthesis in Chlamydomonas via regulation of the *VTC2* gene encoding a GDP-L-galactose phosphorylase. J. Biol. Chem. **287:** 14234–14245.

Vargas, J.D., Herpers, B., McKie, A.T., Gledhill, S., McDonnell, J., van den Heuvel, M., Davies, K.E., and Ponting, C.P. (2003). Stromal cell-derived receptor 2 and cytochrome b_{561} are functional ferric reductases. Biochim. Biophys. Acta **1651:** 116–123.

Vashisht, A.A., et al. (2009). Control of iron homeostasis by an iron-regulated ubiquitin ligase. Science **326:** 718–721.

Wang, Y., Duanmu, D., and Spalding, M.H. (2011). Carbon dioxide concentrating mechanism in *Chlamydomonas reinhardtii*: Inorganic carbon transport and CO_2 recapture. Photosynth. Res. **109:** 115–122.

Whelan, S., and Goldman, N. (2001). A general empirical model of protein evolution derived from multiple protein families using a maximum-likelihood approach. Mol. Biol. Evol. **18:** 691–699.

Wykoff, D.D., Grossman, A.R., Weeks, D.P., Usuda, H., and Shimogawara, K. (1999). Psr1, a nuclear localized protein that regulates phosphorus metabolism in *Chlamydomonas*. Proc. Natl. Acad. Sci. USA **96:** 15336–15341.

Yadavalli, V., Jolley, C.C., Malleda, C., Thangaraj, B., Fromme, P., and Subramanyam, R. (2012). Alteration of proteins and pigments influence the function of photosystem I under iron deficiency from *Chlamydomonas reinhardtii*. PLoS ONE **7:** e35084.

Yagisawa, F., Nishida, K., Yoshida, M., Ohnuma, M., Shimada, T., Fujiwara, T., Yoshida, Y., Misumi, O., Kuroiwa, H., and Kuroiwa, T. (2009). Identification of novel proteins in isolated polyphosphate vacuoles in the primitive red alga *Cyanidioschyzon merolae*. Plant J. **60:** 882–893.

Yamano, T., and Fukuzawa, H. (2009). Carbon-concentrating mechanism in a green alga, *Chlamydomonas reinhardtii*, revealed by transcriptome analyses. J. Basic Microbiol. **49:** 42–51.

Yamasaki, H., Hayashi, M., Fukazawa, M., Kobayashi, Y., and Shikanai, T. (2009). *SQUAMOSA* Promoter Binding Protein-Like7 is

a central regulator for copper homeostasis in *Arabidopsis*. Plant Cell **21:** 347–361.

Yang, T.J., Lin, W.D., and Schmidt, W. (2010). Transcriptional profiling of the Arabidopsis iron deficiency response reveals conserved transition metal homeostasis networks. Plant Physiol. **152:** 2130–2141.

Yuan, Y., Wu, H., Wang, N., Li, J., Zhao, W., Du, J., Wang, D., and Ling, H.Q. (2008). FIT interacts with AtbHLH38 and AtbHLH39 in regulating iron uptake gene expression for iron homeostasis in Arabidopsis. Cell Res. **18:** 385–397.

Yuan, Y.X., Zhang, J., Wang, D.W., and Ling, H.Q. (2005). *AtbHLH29* of *Arabidopsis thaliana* is a functional ortholog of tomato *FER* involved in controlling iron acquisition in strategy I plants. Cell Res. **15:** 613–621.

Zaharieva, T.B., and Abadía, J. (2003). Iron deficiency enhances the levels of ascorbate, glutathione, and related enzymes in sugar beet roots. Protoplasma **221:** 269–275.

Zhang, D.L., Su, D., Bérczi, A., Vargas, A., and Asard, H. (2006). An ascorbate-reducible cytochrome b_{561} is localized in macrophage lysosomes. Biochim. Biophys. Acta **1760:** 1903–1913.

Zheng, L., Huang, F., Narsai, R., Wu, J., Giraud, E., He, F., Cheng, L., Wang, F., Wu, P., Whelan, J., and Shou, H. (2009). Physiological and transcriptome analysis of iron and phosphorus interaction in rice seedlings. Plant Physiol. **151:** 262–274.